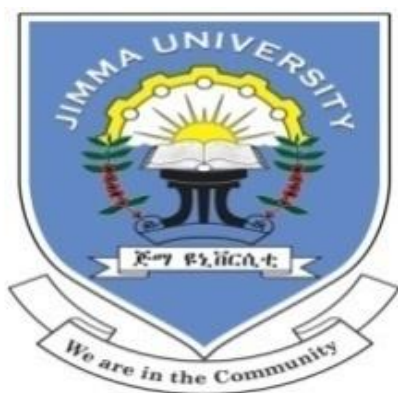


JIMMA UNIVERSITY
SCHOOL OF GRADUATE STUDIES
COLLEGE OF NATURAL SCIENCES
DEPARTMENT OF CHEMISTRY



MSc THESIS ON:

***OCIMUM LAMIIFOLIUM* LEAF EXTRACT SUPPORTED SYNTHESIS OF Ag/CuO
NANOCOMPOSITE FOR PHOTOCATALYTIC AND ANTIBACTERIAL
APPLICATIONS**

BY: TAMIRAT BIRHANU

ADVISOR: GUTA GONFA (PhD)

CO-ADVISOR: GEBRU G/TSADEK (PhD Student)

NOVEMBER 2021

JIMMA, ETHIOPIA

OCIMUM LAMIIFOLIUM LEAF EXTRACT SUPPORTED SYNTHESIS OF Ag/CuO
NANOCOMPOSITES FOR PHOTOCATALYTIC AND ANTIBACTERIAL APPLICATIONS

A THESIS SUBMITTED TO JIMMA UNIVERSITY, SCHOOL OF GRADUTE STUDIES IN
PARTIAL FULFILMENT OF THE REQUIRMENTS FOR THE DEGREE OF MASTERS OF
SCIENCE IN CHEMISTRY (INORGANIC CHEMISTRY)

By: TAMIRAT BIRHANU

ADVISORS: GUTA GONFA (PhD)

GEBRU G/TSADIK (PhD Student)

NOVEMBER 2021
JIMMA, ETHIOPIA

Ocimum Lamiifolium Leaf Extract Supported Synthesis of Ag/CuO Nanocomposites For Photocatalytic and Antibacterial Applications

By: Tamirat Birhanu

A Thesis Submitted to Jimma University, School of Graduate Studies in Partial Fulfilment of the Requirements for the Degree of Masters of Science in Chemistry (Inorganic Chemistry)

Approved by Board of Examiners

Principal Adviser

Signature

Date

Co-Adviser

Internal Examiner

External Examiner

Chairperson

Head of the department

November 2021

Jimma, Ethiopia

TABLE OF CONTENTS

Contents	Page
LIST OF TABLES	IV
LIST OF FIGURES	V
ABBREVIATIONS AND ACRONYMS	VI
ACKNOWLEDGMENTS	VII
ABSTRACT	VIII
Graphical Abstract	IX
1. INTRO DUCTION	1
1.1. Background of the study	1
1.2. Statement of the Problem	4
1.3. Objectives	5
1.3.1. General Objective	5
1.3.2. Specific Objectives	5
1.4. Significance of the Study	5
2. REVIEW OF RELATED LITERATURES	6
2.1. Water pollution and Multi drug resistant bacteria (MDR) with their solution.....	6
2.2. Nanomaterial and Nanotechnology	7
2.3. Synthetic Methods of Nanoparticles and Nanocomposites.....	8
2.3.1. Advantage of plant mediated synthesis of nanoparticles and nanocomposites	9
2.4. Application of nanoparticles, nanocomposites and nanotechnology	10
2.4.1. Principle of photocatalytic activity of nanomaterials	11
2.4.2. Principle of antibacterial activity of nanomaterials	12
2.5. Characterization technique for nanoparticles and nanocomposites	13
2.5.1. UV-Vis spectroscopy.....	13
2.5.2. Fourier Transformation Infrared (FT-IR) Spectroscopy	14
2.5.3. X-ray diffraction (XRD).....	14
2.5.4. Scanning Electron Microscopy.....	14
3. MATERIALS AND METHODS.....	16
3.1. The Study Area.....	16
3.1.1. Materials	16

3.1.2. Chemicals	16
3.1.3. Instruments	16
3.1.4. Sample Collection and Preparation	16
3.2. Preliminary Phytochemicals screening of the <i>Ocimum lamiifolium</i> Plant Extract	17
3.2.1. Test for phenols	17
3.2.2. Test for alkaloids	17
3.2.3. Test for saponins.....	17
3.2.4. Test for flavonoids.....	17
3.2.5. Test for steroids	17
3.3. Synthesis of CuO NPs	17
3.4. Synthesis of Ag doped CuO nanocomposites	18
3.5. Characterizations of the Synthesized CuO NPs and Ag/CuO NCs.....	18
3.6. Application of Synthesized CuO NPs and Ag doped CuO NCs	19
3.6.1. Photocatalytic activity study.....	19
3.6.2. Point of zero-charge analysis (PZC).....	20
3.6.3. Reusability test of the Ag/CuO NCs.....	20
3.6.4. Antibacterial activity	20
4. RESULT AND DISCUSSION	22
4.1. Preliminary Phytochemical Screening of the <i>Ocimum lamiifolium</i> Plant Extract	22
4.2. Synthesis of CuO nanoparticles and Ag/CuO nanocomposites	23
4.3. Parameters Optimization for the Synthesis of Ag/CuO NCs	23
4.3.1. Concentration of $\text{Cu}(\text{NO}_3)_2 \cdot 3\text{H}_2\text{O}$ optimization	23
4.3.2. Plant extract optimization.....	24
4.3.3. Concentration of dopant optimization	24
4.3.4. Effect of pH	25
4.3.5. Effect of temperature	26
4.3.6. Effect of reaction time	26
4.4. Characterization of Synthesized CuO Nanoparticles and Ag/CuO Nanocomposites	27
4.4.1. UV-Vis spectroscopy Analysis.....	27
4.4.2. FT-IR Analysis	29
4.4.3. X-Ray Diffraction Analysis.....	30
4.4.4. Scanning Electron Microscopy (SEM) analysis.....	32

4.5. Application of synthesized CuO NPs and Ag/CuO NCs	33
4.5.1. Photocatalytic activity of Ag/CuO NCs	33
4.5.2. Optimization of parameters for the photocatalytic degradation of MB.....	33
4.6. Reusability of the photocatalyst	41
4.7. Antibacterial Activity.....	43
CONCLUSION AND RECOMMENDATIONS	46
5.1. Conclusion.....	46
5.2. Recommendation.....	47
6. REFERENCES	48
LIST OF APPENDICES.....	59

LIST OF TABLES

Table 1: Summary of plants utilized for the synthesis of Ag/CuO NCs.....	10
Table 2: Phyto-chemical components of <i>ocimum lamiifolium</i> plant extract	22
Table 3: Effect of CuO NPs on selected bacteria (<i>Salmonella typhaea</i> , <i>Bacillus cereus</i> , <i>staphylococcus aureus</i> , and <i>Escherichia coli</i> at different concentrations.	43
Table 4: Effect of Ag/CuO NCs on selected bacteria's (<i>Salmonella typhaea</i> , <i>Bacillus cereus</i> , <i>staphylococcus aureus</i> and <i>E.coli</i>) at different concentrations.....	43

LIST OF FIGURES

Figure 1: <i>Ocimum lamiifolium</i> plant.....	3
Figure 2: Impacts of textile dye effluent.....	6
Figure 3: Top-down and Bottom-Up Approaches in Synthesizing Nanomaterials	9
Figure 4: Application of nanotechnology	10
Figure 5: Principle of photocatalytic process.....	12
Figure 6: NM antibacterial mode of action.....	13
Figure 7: Chemical structure of Methylene blue dye (MB).....	19
Figure 8: UV-Vis spectra of (a) CuO NPs (b) Ag/CuO NCs.....	27
Figure 9: The tauc plot of (a) CuO NPs (b) Ag/CuO NCs.....	28
Figure 10: FT-IR spectra of (a) Plant extract (b) CuO NPs (c) Ag/CuO NCs.....	30
Figure 11: XRD spectra of CuO NPs and Ag/CuO NCs	32
Figure 12: SEM image of (a) CuO NPs (b) Ag/CuO NCs.....	33
Figure 13: (a) Dark absorption-desorption equilibration (b) Effect of catalyst dosage and contact time on the degradation of MB dye [MB=10 mg/mL, Ag/CuO NCs (20-50 mg)].....	34
Figure 14: Surface charge of Ag/CuO NPS	35
Figure 15: Effect of pH on the degradation of MB dye (MB=10 mg/mL at 120 min).....	36
Figure 16: Effect of irradiation time on the degradation of MB using (a) Ag/CuO NCs and (b) CuO NPs at different time interval, (MB=10 mg/L, pH 9) under LED lamp, 200 W irradiation.....	37
Figure 17: Effect of irradiation time on the degradation of MB dye without catalyst.....	38
Figure 18: Effect of irradiation time on the degradation of MB dye (30 mg Ag/CuO NCs, MB=10 mg/L, pH 9) by Ag/CuO NCs at different time intervals under sunlight irradiation.....	39
Figure 19: Effect of the initial concentration of MB dye on the degradation efficiency (%) at pH 9 and 30 mg Ag/CuO NCs	41
Figure 20: Reusability test of Ag/CuO NCS	42

ABBREVIATIONS AND ACRONYMS

CB	Conduction Band
COVID-19	Corona virus infectious disease
DI	Deionized water
DNA	Deoxyribonucleic acid
Eg	Energy bandgap
FT-IR	Fourier transformed infrared
MB	Methylene Blue
MDR	Multi-drug Resistant
NCs	Nanocomposites
NM	Nanomaterial
NPs	Nanoparticles
PXRD	Powder X-Ray Diffraction Analysis
ROS	Reactive Oxygen Species
RNA	Ribonucleic Acid
RNS	Reactive Nitrogen Species
SEM	Scanning electron microscopy
SPR	Surface Plasmon resonance
TG/DTA	Thermo-Gravimetric/Differential Thermal Analyzer
TEM	Transmission Electron Microscopy
UV–Vis	Ultraviolet-Visible
VB	Valance Band

ACKNOWLEDGMENTS

First, I would like to give the greatest possible glory and thank to my almighty God, for being with me through all my work. Next, I would like to thank my advisors Dr. Guta Gonfa and Mr. Gebru G/Tsadik and all JU chemistry staff members for their scientific guidance, support and motivating me during the preparation of this research work.

Additionally, I would like to acknowledge Mr. Demelash Jado, Rada Namo, and Regassa Belachew for their unreserved support during my research work. Lastly, I am grateful to all my family especially my mother and father for continuous praying, and my brother Sagni Biranu for his guidance and support during my study time.

ABSTRACT

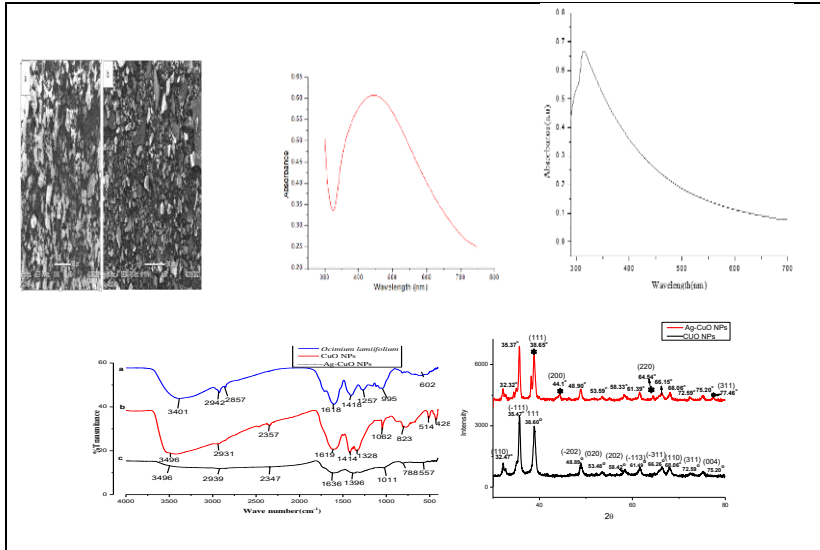
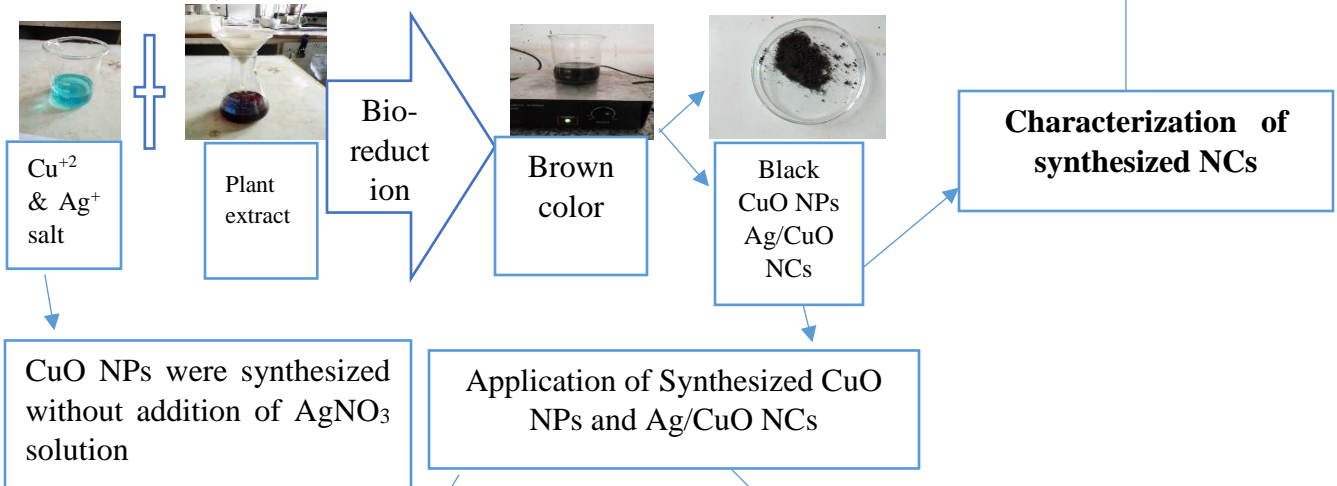
Since dye effluents discharged from different industries lead to environmental contamination, their treatment and remediation method is highly desired. Due to the limitation of physical methods like adsorption, the photocatalytic degradation method was used because of its capability to complete the degradation of dyes. On the other hand, most bacteria have shown resistance to antibiotic drugs. In this regard, nanomaterial has been found to be a promising candidate to overcome the problem of antibiotic (drug) resistance. The main objective of this research was to synthesize CuO NPs and Ag doped CuO NCs by using *Ocimum lamiifolium* plant extract by precipitation method for photocatalytic and antibacterial applications. Ag/CuO NCs were prepared from *ocimum lamiifolium* leaf extract, copper nitrate trihydrate, and silver nitrate solution at 70 °C. CuO NPs were synthesized in the same way but without addition of silver nitrate solution. The synthesized CuO NPs and Ag/CuO NCs were characterized by using UV-Vis, XRD, SEM, and FT-IR. From UV-Vis absorption spectrum, the peaks of CuO NPs and Ag/CuO NCs were detected at 308 and 452 nm with E_g of 2.56 and 1.84 eV respectively. FT-IR revealed the presence of carbonyl and hydroxyl groups in the synthesized nanomaterials. The XRD data showed the crystalline structure of CuO NPs and Ag/CuO NCs with crystallite sizes of 29.1 and 38.2 nm respectively. SEM shows some of CuO NPs has a spherical shape and Ag/CuO NCs has a mixture of spherical and rod-like shape. The in-vitro antibacterial test of NPs showed good antibacterial activity, especially at higher concentrations. The result indicates that Ag/CuO NCs showed enhanced antibacterial activity compared to CuO NPs. The photocatalytic performance of Ag/CuO NCs was further assessed by degradation of MB as a model pollutant under visible light (LED lamp, 200 W) irradiation and compared with CuO NPs. The effects of some parameters such as catalyst dosage, contact time, pH, irradiation time, and the effect of initial concentration of MB dye on the activity of the Ag/CuO NCs were also investigated. 88.5 and 76.2% of MB were degraded by Ag/CuO NCs and CuO NPs at 120 min, respectively. The Ag/CuO NCs can also decompose MB in natural sunlight irradiation, and 95.1% was degraded in 60 min, which is promising for future application of solar light-driven photocatalytic degradation of organic pollutants.

Keywords: *CuO NPs, Ag/CuO NCs, Ocimum lamiifolium, Anti-bacterial activity, Photocatalytic activity*

Graphical Abstract

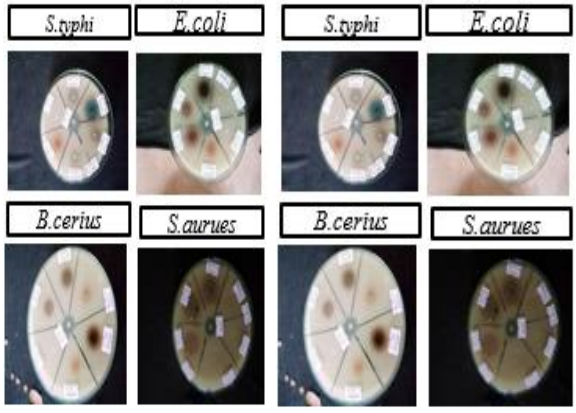


Plant leaves

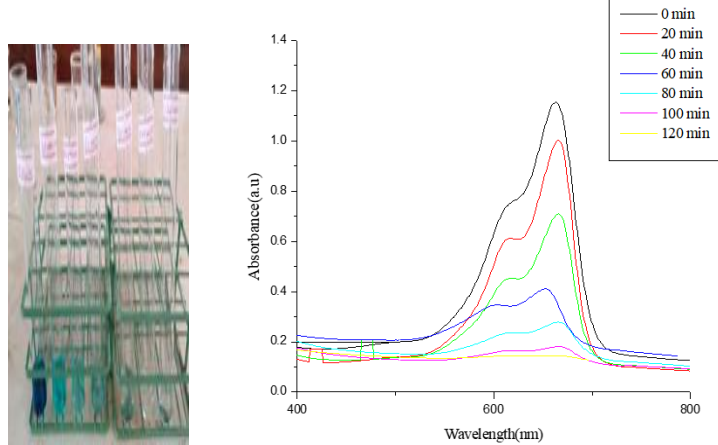


Characterization of synthesized NCs

Antibacterial activity CuO and Ag/CuO NCs



Degradation of MB dye



1. INTRO DUCTION

1.1. Background of the study

Nowadays, the world mostly affected by cancer due to environmental pollution in its one or the other form, out of which water pollution is of prime concern [1]. Textile and paper industries discharge huge amount of aqueous wastes and carcinogenic dye effluents, which is environmentally unacceptable since they can cause environmental damage by causing water pollution. Organic dyes are stable organic pollutants that persist in the environment. Therefore, methods for their degradation have been increasingly explored and developed. Despite the number of successful systems employing various physicochemical and biological processes, economical removal of color from effluents remains a major problem [2]. Therefore, it is necessary to develop better economically and environmentally friendly treatment technologies. Currently, photocatalytic degradation by nanoparticles is attracting significant attention. In photocatalytic degradation, the pollutants degraded under UV-Vis light irradiation in the presence of catalysts. Compared to the conventional methods, this technique is inexpensive and does not form any polycyclic product [3].

Most bacteria cause different health problems on living things. Therefore, in order to overcome this effect of bacteria, antibacterial agents must be required. Antibacterial agents are compounds that kill bacteria or slow down their growth without being generally toxic to the surrounding tissue [4]. However, over-use of antibiotics has led to an increased occurrence of antibiotic resistant genes in various bacterial species. Dealing with antibiotic-resistant bacteria is costly and requires more time and may be associated with side effects and sometimes-therapeutic failure[5, 6].Therefore, researchers are looking for alternative and novel antimicrobial agents [7]. In this case, nanoparticles and nanocomposites have been demonstrated to be a promising application to overcome the problem of antibiotic resistance [8].

Transition metal oxides such as CuO, TiO₂, Fe₃O₄, ZnO, and NiO NPs have shown effective applications as advanced nano-substances into energy, biomedical and environmental fields of study [9]. The strong adsorption capability exhibited by these NPs significantly enhance their performance and applications [10].

Copper oxide nanoparticles (CuO NPs) and their derivatives are widely used in many applications due to fair stability, cost-effectiveness, and readily available [11]. Some of their applications are; catalyst for chemical reactions, solar cell, chemical sensor, adsorbent, thermal conductivity enhancer, wastewater treatment and anti-oxidation properties, drug delivery, anticancer activity, and efficient anti-microbial agent [11, 12].

Different physical and chemical approaches like microwave irradiation, thermal decomposition, sol gel, colloidal thermal synthesis, sonochemical, hydrothermal, and quick precipitation have been employed for the synthesis of CuO NPs with desired morphologies. However, these methods require labor-intensiveness, energy, intensive routes, expensive and hazardous chemicals [9, 13]. Hence, simple, low cost, and green synthesis method for NPs is highly required.

Synthesis of metal or metal oxide nanoparticle using biological approach was found to be potential low cost, green and efficient method [14]. It focus on the utilization of bacteria, fungi, algae, yeast, and plant extracts, as a reducing agent for the synthesis of nanoparticles that support bio-compatibility and large-scale production [15]. From the biological approach of metal or metal oxide nanoparticle synthesis, Phyto-synthesis or plant-mediated nanoparticle synthesis has gained more attention due to an inexpensive method, time-effective, and cost-effective than the other biological methods [16]. Therefore, Phyto-synthesis has become an upcoming profitable alternative for large-scale production.

Primarily metal oxides with different band gaps are common photocatalysts for environmental remediation. However, for most metal oxides the recombination between the excited electrons and holes in the semiconductor could hinder their photocatalytic activity [16]. Therefore, to get enhanced photocatalytic activity, a reduction in recombination rate must be required. Furthermore, metals like those that (Ag, Au, Fe, Cu, Ru, and Pd) deposited on metallic oxide surfaces has gained considerable attention since they can play a significant role to improve the photocatalytic efficiency of nanoparticles by reducing electron re-combination rate [17]. Now, doping in CuO has been significantly investigated since their properties can be simply controlled by suitable dopants. CuO/noble metal nanocomposites could efficiently decrease the photo-generated electron-hole recombination because the photo-generated electrons accumulate on the

metal, and holes stay behind on the CuO surface [17]. Ag have gained particular attention because of their high electrical conductivity along with excellent oxidation stability [18]. Therefore, Ag was chosen to be doped with CuO nano particles to form Ag doped CuO nanocomposites, and its enhanced properties was studied.

The genus *Ocimum* (*Lamiaceae*) consists of about 30 Old and New worlds, with some species cultivated in temperate areas. *Ocimum lamiifolium* (Damakase, Amharic local name) is mostly found in clearings and edges of primary and secondary mountain forests and bush lands, tall grasslands, abandoned fields, at altitudes between 1200 and 2900 m. Traditionally, the fresh leaves are squeezed and the juice is sniffed to treat cough, cold, relieve pain, wound, fever, malaria and inflammatory disorders in Ethiopia, and the juice is also used as eye rinse to treat eye infections. At the same time, the crushed leaves are put in the nostrils to stop nose bleeding [19]. The secondary metabolites present in *Ocimum lamiifolium* (Fig. 1) are alkaloids, flavonoids, saponins, and tannins [20]. During synthesis of CuO NPs and Ag/CuO nanocomposites, these secondary metabolites can act as a reducing as well as a capping agent [21].



Figure 1: *Ocimum lamiifolium* plant

Recently, the synthesis of CuO NPs and Ag/CuO NCs using *Malus Domestica*, *Muntingia calabura*, *Cyperus Pangorei*, and *Mimosa Pigra* plant extract has been reported [22, 23, 41, 42]. However, utilization of *Ocimum lamiifolium* for the synthesis of CuO NPs and Ag/CuO NCs was not reported yet. Inspired by the above facts, here we prepared Ag/CuO NCs and investigated their photocatalytic activity in comparison to CuO NPs. Furthermore, the antibacterial activity of Ag/CuO nanocomposites against two gram-positive bacteria (*Staphylococcus aureus* and *Bacillus cereus*) and two gram-negative bacteria (*Salmonella typhi* and *Escherichia coli*) were investigated, and compared with that of bare CuO.

In this study, the synthesis of CuO NPs and Ag/CuO NCs utilizing the *Ocimum lamiifolium* leaf extract has been addressed for the first time. The synthesized Ag/CuO NCs and CuO NPs were characterized by UV–Vis, FT-IR, XRD, and SEM techniques. This biosynthesized visible-light photocatalyst was used for the degradation of Methylene blue (MB) dye as a model pollutant. The various factors that affect the catalytic activity has been investigated. The antibacterial application of synthesized nanomaterials was also assessed.

1.2. Statement of the Problem

The release of colored dyes like methylene blue (MB) into the environment has been of great concern due to the properties and effects of dye-contaminated water on the environment. Dye contaminated wastewater disposal is of prime concern because it is toxic to humans and aquatic life. These dyes are not biodegradable and cause water pollution and serious long-term effects on the environment. Therefore, to minimize the health effects of these pollutants, treatment methods need to be studied. Methods of removal of these dyes such as adsorption by activated charcoal are not effective; since they result in large amounts of sludge which can cause pollution problems again. Therefore, photocatalysis has been proven to be a more efficient method for the degradation of MB. However, some of the photocatalysts like CuO NPs have high rate of recombination of the photogenerated electrons. To overcome this limitation of CuO photocatalyst, doping with some other metal is required to enhance photocatalytic activity by reducing re-combination rate. Additionally, antibiotic drug-resistant bacteria become lead to serious health problems caused by overuse or misuse of the medication. Consequently, the synthesis of CuO NPs and Ag/CuO NCs is strongly required to remove toxic dyes to remediate a safe environment and fill the gaps in which antibacterials are frequently failed. However, the physical and chemical methods of synthesis of nanoparticles are expensive and not eco-friendly. Having the above pieces of evidence, the present study was intended to explore the photocatalytic activity of *Ocimum lamiifolium* leaf extract supported CuO NPs and Ag/CuO NCs and evaluation of their antibacterial activities. Even though CuO NPs and Ag/CuO nanocomposites were synthesized by using some plant extracts [22, 23], utilization of *Ocimum lamiifolium* extract as a capping and reducing agent was not reported yet. Based on the above facts, this study may answer the following questions:-

- Is *Ocimum lamiifolium* leave extract as reducing and capping agent for the synthesis of CuO NPs and Ag doped CuO NCs.
- Do the synthesized nanoparticles and nanocomposites show enhanced activity than that of plant extract or other nanoparticles synthesized before or from the literature?
- Do CuO NPs and Ag doped CuO NCs show good photocatalytic and antibacterial applications?

1.3. Objectives

1.3.1. General Objective

The main objective of this study is to synthesize Ag doped CuO nanocomposites using *Ocimum lamiifolium* leaf extract and evaluate photocatalytic and antibacterial applications.

1.3.2. Specific Objectives

- To prepare *Ocimum lamiifolium* leaf extract.
- To conduct phytochemical screening test.
- To synthesize CuO NPs and Ag doped CuO NCs using *Ocimum lamiifolium* leave extract as reducing and capping agent.
- To characterize the synthesized CuO NPs and Ag doped CuO NCs using UV-Vis spectrophotometer, FT-IR, XRD, and SEM.
- To evaluate photocatalytic and antibacterial applications of the Ag doped CuO NCs and comparing with CuO NPs.

1.4. Significance of the Study

The green synthesis of nanoparticles using plant extract is an active area of current research, attracting the interest of many researchers because of their wide applications. Nowadays due to expansion of water pollution and multidrug resistant bacteria, synthesis of nanoparticle is highly important. Therefore, the finding of this study was used:

- To enhance the knowledge about CuO NPs and Ag doped CuO NCs regarding their antibacterial and photocatalytic applications.
- To set foundation for further investigation of applications of CuO NPs and Ag doped CuO NCs.

2. REVIEW OF RELATED LITERATURES

2.1. Water pollution and Multi drug resistant bacteria (MDR) with their solution

Water pollution is one of the major problems worldwide and the most important cause of diseases and deaths [24]. There are different types of the factor responsible for the polluting the natural water bodies such as mining activities, urbanization, and fast industrialization. Among all the factors, fast industrialization mainly textile, food processing, paper, and dye manufacturing industries are the major sources of water pollution. The wastewater from those industries is extremely charged with unconsumed dyes and traces of metals. These discharges cause major destruction to the environment [25, 26] (Fig. 2).

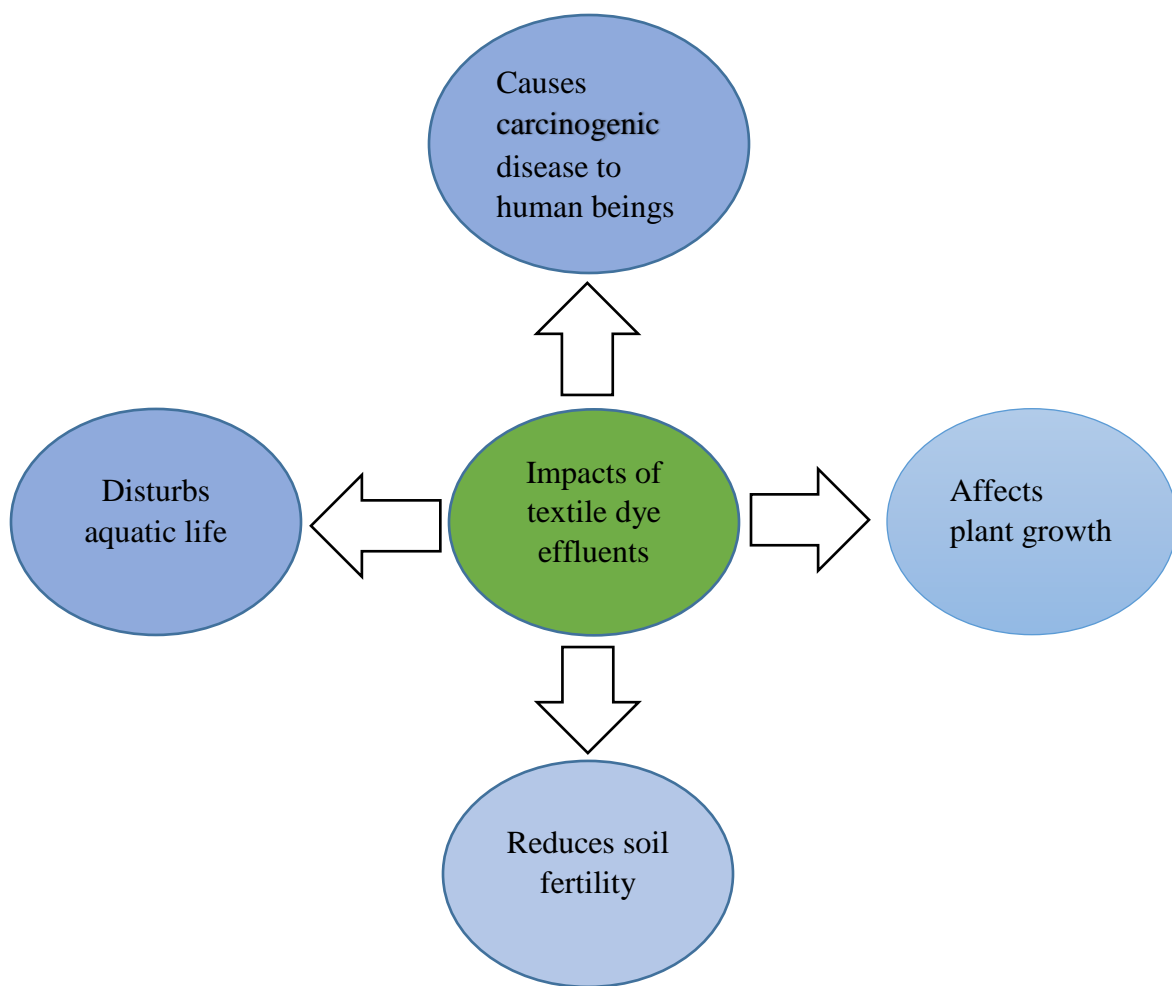


Figure 2: Impacts of textile dye effluent

Therefore, everywhere researchers are looking for proper management to get rid of these pollutants and to achieve degradation of dye house effluents.

At present, several techniques have been developed for the removal of pollutants from wastewater, such as adsorption, chemical coagulation, filtration, sedimentation, but they are not economical and can cause secondary pollution to the environment [27]. Recently, photocatalytic degradation is gaining significant importance due to its ability to generate a sufficient number of highly reactive radicals for effective water decontamination and its capability of converting organic pollutants into non-toxic species (CO_2 and H_2O) [28, 29].

Antibiotic resistance is a serious public health problem that are capable of causing serious disease with high mortality, disease, and high cost of treatment [30]. Drug-resistant bacteria have emerged because of the misuse of antibacterial medications. Examples of antibiotic resistant bacteria are *Staphylococcus aureus*, *Escheria coli*, *Bacillus cereus*, *Salmonella typhi* and etc. Antibiotic resistant bacteria cause a great problem for the efficient management of bacterial infections and this challenge has resulted in the creation of other means of dealing with bacterial diseases. Of late, nanoparticles and nanocomposites employed as antibacterial agents and have the potential to overcome the effect of antibiotic resistant bacteria [31].

2.2. Nanomaterial and Nanotechnology

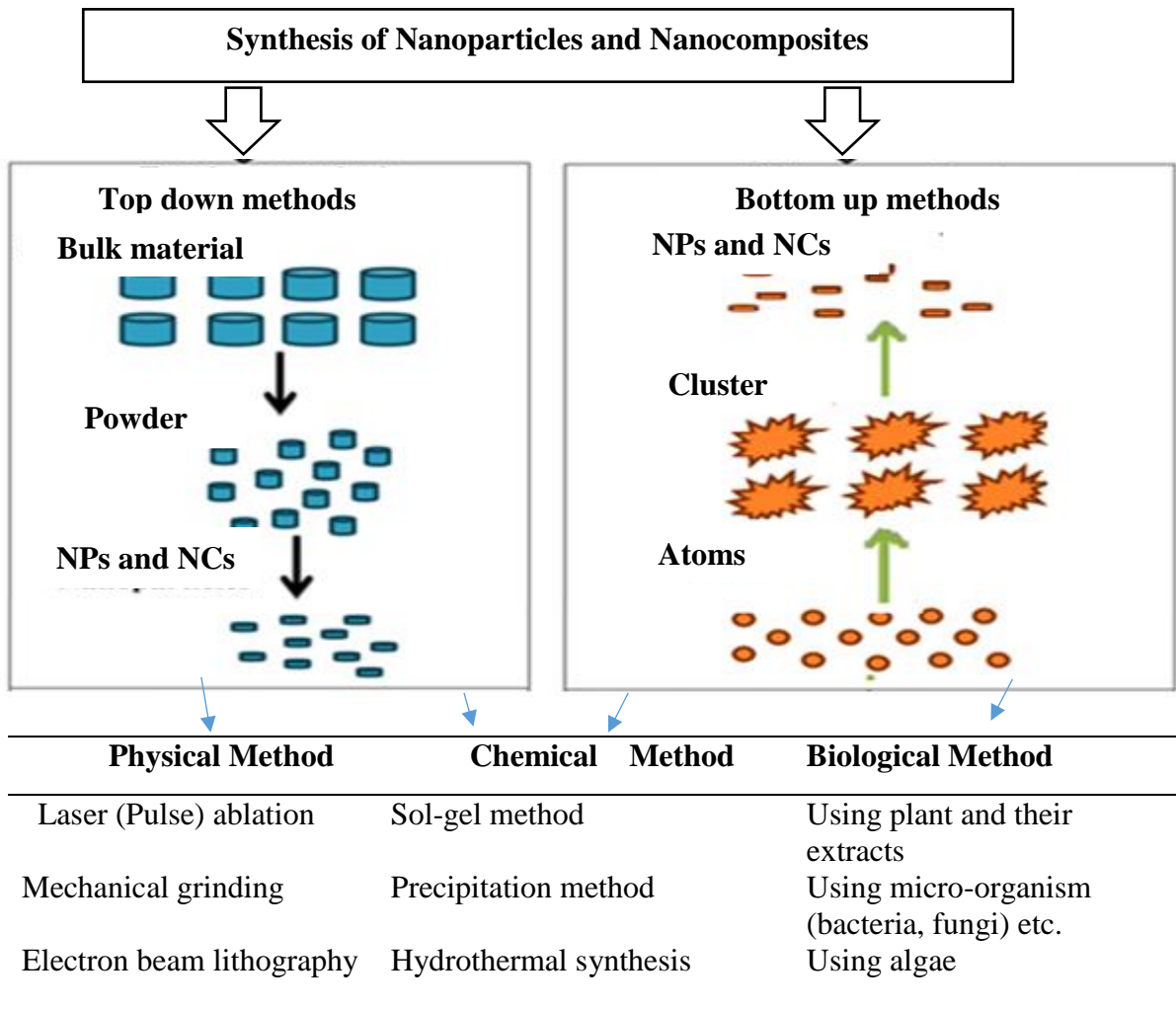
Nanotechnology is a field of science and technology which deals with production, manipulation and use of materials that are in nanometers [32]. The advances in nanotechnology have led to the greater development in various fields, including nanoparticles, nanotubes, and nanowire synthesis. Nanomaterials are particles (crystalline or amorphous) of organic or inorganic materials having sizes in the range of 1-100 nm. To distinguish nanomaterials from bulk, it is vitally important to demonstrate the unique properties of nanomaterial's and their prospective impacts in science and technology [33]. Properties of nanometric dimensions are significantly different from those of atoms as well as those of bulk materials. Suitable control of the properties of nanometer-scale structures can lead to new science as well as new devices and technologies [34]. Nanomaterials have properties that are significantly different and considerably improved relative to those of their bulk counterparts. The property changes is due to their large surface areas and small grain sizes of nanomaterial's [35].

2.3. Synthetic Methods of Nanoparticles and Nanocomposites

Nanoparticles and nanocomposites can be formed by two approaches: top-down (comminution and dispersion) or bottom-up (nucleation and growth) (Fig. 3).

The top-down approach is making use of the starting bulk materials of the same materials that going to be synthesized and applying energy to break down the large materials into smaller fragments. Sources of energy can be mechanical, thermal, or chemical.

However, there is a disadvantage associated with this method whereby creating particles with wide size distribution [36]. To overcome this limitation, the bottom-up method was introduced as it is considered simpler and more favorable in synthesizing particles in size less than 100 nm. It was like building the atoms one by one, first started with a simple metal salt, slowly converts it from ions to elemental atoms and grown in the form of nano-size particles [37].



Spray pyrolysis	Thermal decomposition	Using enzymes and bio-molecules
Mechanical milling and etc.	Electrochemical method and etc.	Using industrial and agricultural wastes

Figure 3: Top-down and Bottom-Up Approaches in Synthesizing Nanomaterials

The synthesis approach of NPs and NCs in general can be classified as physical, chemical and biological methods. CuO NPs and Ag/CuO NCs can be synthesized by various chemical methods such as sol-gel method, precipitation, hydrothermal synthesis, chemical reduction, thermal decomposition, electrochemical method and wet chemical method [38]. Nevertheless, chemical methods for nanomaterial synthesis are associated with various disadvantages such as expensive, involve the use of hazardous chemicals, time consuming and pose environmental threats by generating toxic solvent and waste products [39]. Therefore, environmentally friendly approach in synthesizing the metal or metal oxide nanoparticles is required. It has been reported that many of the biological systems such as bacteria, fungi, algae and plants can be used to convert metal ions into metal nanoparticles and from biological synthesis method, Plant based preparation has become common due to its simple, comprehensive availability and extensive range of samples including plant part extracts and natural products. In addition, plant leaf core, root, latex seed and stem contain poly-phenol and have been successfully used for metal or doped metal oxide nanocomposite synthesis [40].

2.3.1. Advantage of plant mediated synthesis of nanoparticles and nanocomposites

The use of plants or plant extracts which act as reducing and capping agents for NM synthesis is more useful over other biosynthesis procedures. Because, in this technique no need of cell culturing and cell maintenance. Moreover, nanomaterials synthesized from plants is more stable and allows the production of NPs with different shapes and sizes, and is cheap [41]. The phyto-synthesized nanoparticles such as Ag, Au, Pt, Cu are widely used in bio-medicine, pharmaceuticals, bio-labelling, food packaging, cosmetics, catalysis and sensory applications [42]. Even though, CuO NPs were synthesized by large number of plant extract, Ag/CuO NCs synthesized by plant extract is rare. Therefore, some of the plants used for the synthesis Ag/CuO NCs were listed in the table below.

Table 1: Summary of plants utilized for the synthesis of Ag/CuO NCs

Name of plant	Size (nm)	shape	Application	References
<i>Cyperus pangorei</i>	27.24	Spherical	Photocatalytic degradation	[43]
<i>Mimosa pigra</i>	49.5	Spherical	Photocatalytic degradation	[44]
<i>Malus domestica</i>	20	Spherical	Antibacterial and antioxidant	[45]
<i>Muntingia calabura</i>	24	Irregular	Antimicrobial applications	[23]

2.4. Application of nanoparticles, nanocomposites and nanotechnology

Nanotechnology plays a very important role in modern research due to its huge application in many fields such as pharmacy, water purifications, health, biomedical sciences, pharmaceuticals, chemistry and chemical industry, sensor, environmental health, and antimicrobial applications [46] (Fig. 4).

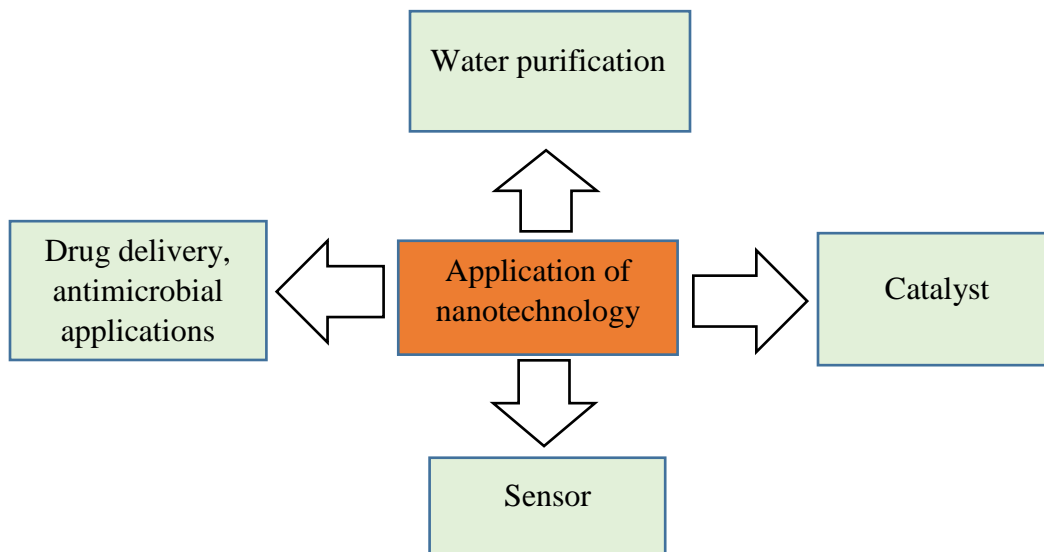


Figure 4: Application of nanotechnology

Among these wide applications, using metal oxide nanoparticles have found considerable results in several applications including nanochemistry [47].

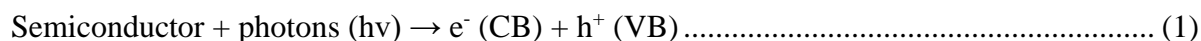
Potential technological applications of metal oxide nanoparticles play a vital role and attracting researchers with considerable interest from the fields of materials chemistry, medicine, agriculture, information technology, biomedical, optical, electronics, catalysis, environment, energy, and sensor [48].

Consequently, nanosized metal oxide materials are of considerable interest because of significant advantages over bulk analogue because they have great prospects for obtaining new types of adsorbents, photo-catalysts, and sensitive layers of gas sensors based on them. However, metal oxides also have a significant drawback. Example fast electron-hole recombination during photo-catalysis [49].

In this case, it is promising to create doped metal oxide nanocomposite as an extremely interesting type of nanomaterial due to their applications that may exceed the application of its corresponding nanomaterials. Metal/metal oxide nanocomposites are known to lead to enhanced efficiency in photocatalytic degradation [50]. In addition, metal-doped metal oxide nanocomposites due to their special and unique physical and chemical properties, they can be applied in a wide variety of fields, including the production of new materials in the fields of medicine, antimicrobial activity, energy, and ecology [51]. Additionally, they have excellent antiviral activities like in the treatment of coronavirus (COVID-19) [52]. Generally, nanoparticles and nanocomposites are widely used in photocatalytic and antibacterial applications in which their principle is explained below.

2.4.1. Principle of photocatalytic activity of nanomaterials

When the semiconductor is illuminated by photon energy equal to or greater than the band-gap energy (E_g), it excites electrons (e^-) from the VB to CB. Simultaneously, it causes the formation of a positive charge called a hole (h^+) in the valence band and electron at the conduction band [50]. The photogenerated positive holes react with water to produce hydroxyl radicals ($\cdot OH$) while the photogenerated electrons react with oxygen and produce superoxide radicals ($O_2^{\cdot-}$). Both of these primary products (specifically $\cdot OH$ radicals) are strong oxidizing species that attack organic pollutants such as MB and decomposes them into CO_2 and H_2O [53, 54] (Fig. 5) and their reaction is as shown as equation below.



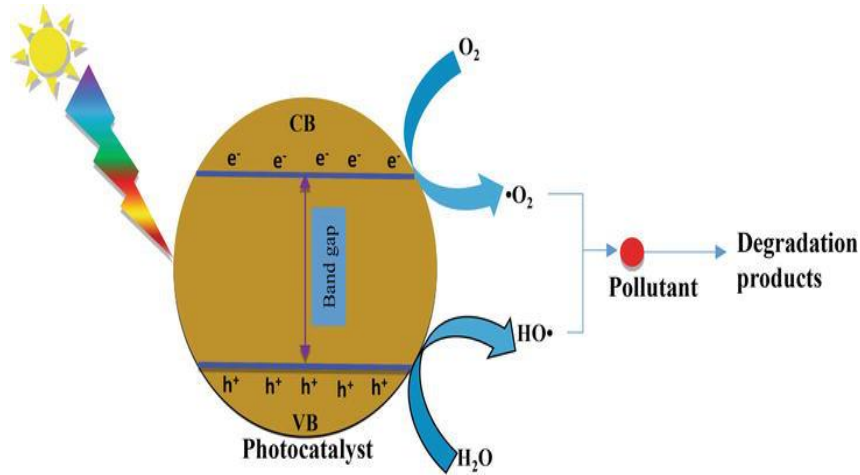
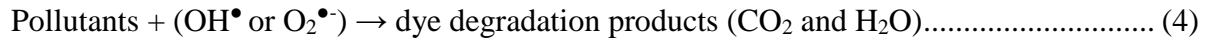


Figure 5: Principle of photocatalytic process

2.4.2. Principle of antibacterial activity of nanomaterials

Different types of nanomaterials and nanocomposites have different mechanisms for combating antibiotic resistant bacteria [55]. Nevertheless, nanomaterials act along two major lethal pathways, which are related to each other and in many cases occur simultaneously: (a), free metal ion toxicity arising from dissolution of the metals from surface of the nanoparticles and (b), oxidative stress via the generation of reactive oxygen species (ROS) on surfaces of the nanomaterials [56].

Cell wall disruption and membrane damage and occurs when NM bind electrostatically to the bacterial cell wall and membranes, leading to alteration of membrane potential, membrane depolarization, and loss of integrity which result in an interruption of electron transport, impaired respiration, interruption of energy transduction or cell lysis, and eventually cell death [55]. ROS is considered as the most effective determinant for both *in vitro* and *in vivo* cytotoxicity of NM. A burst of ROS causes via severe oxidative stress, damage to all the cell's macromolecules, leading to lipid peroxidation, alteration of proteins, inhibition of DNA replication, protein denaturation, and DNA damage. At high concentrations, the ROS lead to cell death and at low doses cause severe DNA damage and mutations [57, 58].

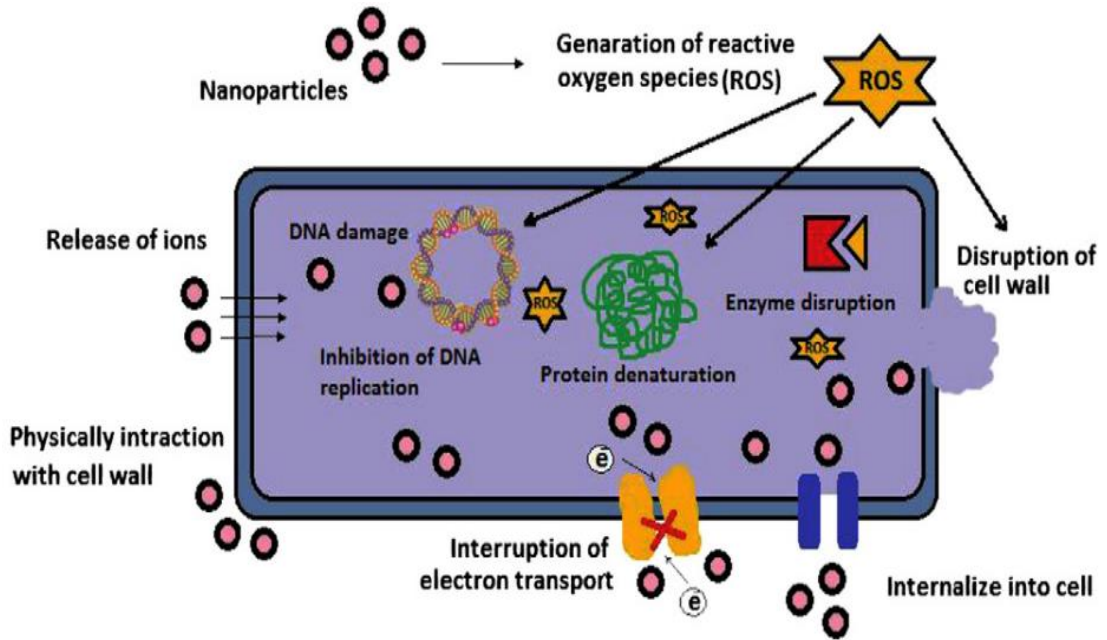


Figure 6: NM antibacterial mode of action

2.5. Characterization technique for nanoparticles and nanocomposites

2.5.1. UV-Vis spectroscopy

The Principle of UV-Visible Spectroscopy is based on the absorption of ultraviolet light or visible light by chemical compounds, which results in the production of distinct spectra. UV-Vis spectroscopy used to show band gap energy of synthesized nanomaterials. The band gap energy (E_g) of the synthesized nanomaterial can be obtained by using equation 5 [59]

$$E_g = \frac{1240}{\lambda} \text{ eV} \dots\dots\dots(5)$$

Where E_g is the band gap in electron volt (eV) and λ is the wave length of the absorption edges in the spectrum in nano mater (nm). The band gap increases with decreasing particle size and the absorption edge is shifted to a higher energy (blue shift) with decreasing particle size [60]

In this study the energy band gap were calculated by using tauc plot. Tauc plot has the photon energy ($h\nu$) on the X axis and a quantity $(\alpha h\nu)^2$ on the Y axis and extrapolating the linear portion of the curve to the X axis yields the band gap energy of the material [61]. Generally, Surface Plasmon resonance and energy band gap of synthesized of synthesized CuO NPs and Ag/CuO NCs were analyzed by UV-Vis spectroscopy.

2.5.2. Fourier Transformation Infrared (FT-IR) Spectroscopy

FTIR spectroscopy analysis is a method based on the principle of infrared spectroscopy, and it has extended its area of application to the study of nano-scaled objects during the last decade [62].

FT-IR spectroscopy is used to identify the possible functional groups of the active components present in the extracts or on the surface of nanomaterials that are responsible for reducing and stabilization of synthesized nanoparticles and nanocomposites. The possible functional groups that are present in the plant extract and synthesized CuO NPs and Ag/CuO NCs were identified in the ranges of 4000-400 cm^{-1} [63].

2.5.3. X-ray diffraction (XRD)

X-ray diffraction is based on constructive interference of monochromatic X-rays and a crystalline sample. These X-rays are generated by a cathode ray tube, filtered to produce monochromatic radiation, collimated to concentrate, and directed toward the sample [64]. X-ray diffraction (XRD) technique is used to realize structural properties of materials and give information like crystal structure/phase, lattice parameters, crystallite size, orientation of single and poly crystals, defects, strains and so on [65].

The crystallite can be extracted from XRD spectra by analyzing the line profile of the diffraction peak. This was calculated from the most intense peaks using Debye- Scherer's formula below

$$D = \frac{k\lambda}{\beta \cos\theta} \dots\dots\dots(6)$$

Where, D is crystallite size in nanometer, k is shape factor constant, which is 0.89, β is the full width at half maximum (FWHM) in radian, λ is the wavelength of the X-ray and θ is the Bragg angle [66].

2.5.4. Scanning Electron Microscopy

The SEM instrument is based on the principle that the primary electrons released from the source provide energy to the atomic electrons of the specimen, which can then release as the secondary electrons (SEs) and an image can be formed by collecting these secondary electrons from each point of the specimen [67].

The scanning electron microscope (SEM) is a very useful instrument to get information about topography, morphology and composition information of materials. It is a type of electron microscope capable of producing high-resolution images of a sample surface. Due to how the image is created, SEM images have a characteristic three-dimensional appearance and are useful for judging the surface morphology of the sample [68]. The morphology of synthesized CuO NPs and Ag/CuO NCs were analyzed by SEM.

3. MATERIALS AND METHODS

3.1. The Study Area

The study was carried out at Jimma University main campus, Chemistry Research Laboratory which is located at 346 Km away from Addis Ababa, Ethiopia.

3.1.1. Materials

Oven, Mortar and Pestle, Digital balance, Hot Plate and Magnetic bar, Watch, Centrifuge, Filter paper, Beakers, Test tubes, Droppers, Graduated cylinders, Glass rode, Rack, Cuvettes, Refrigerator, Erlenmeyer flask.

3.1.2. Chemicals

Copper nitrate trihydrate [$\text{Cu}(\text{NO}_3)_2 \cdot 3\text{H}_2\text{O}$], Copper(II) sulfate pentahydrate ($\text{CuSO}_4 \cdot 5\text{H}_2\text{O}$, 95%), Silver nitrate (AgNO_3 , 99%), Sodium hydroxide (NaOH ; 99%, Sigma-Aldrich, India), Ethanol (99%, Alfa Aesar, India), Methylene blue (Sigma Aldrich, >99%), Ferric chloride (anhydrated) (FeCl_3), Dilute hydrochloric acid (HCl), Dragendroff's reagent (Bismuth nitrate, $\text{Bi}(\text{NO}_3)_3$; Glacial Acetic Acid(CH_3COOH); Potassium iodide, KI), Deionized water (DI).

3.1.3. Instruments

UV-Vis(Aspect-1.2.3.6173,Analytic jena and UV-Jenway6705), FT-IR (65 FTIR Perkin Elmer), XRD (X-ray diffraction; XPERT-PRO Machine), SEM (transmission electron microscopy) technique.

3.1.4. Sample Collection and Preparation

Ocimum lamiifolium leaf samples were collected from Jimma Zone, around Aba Jifar palace 346 Km away from Addis Abeba. Sample collection and preparation of *Ocimum lamiifolium* leaves extract were carried out according to the procedure written on the reported literatures [20, 69, 70], with slight modifications. *Ocimum lamiifolium* leaves were collected and the collected fresh leaves were washed thoroughly with deionized water to remove any dirty particles. The washed leaves were air-dried and about 3 gm of the grinded leaves along with 100 mL of distilled water was heated in a hot plate at 70 °C for 30 min. After 30 min, it was filtered using Whatmann filter paper having pore size of 11 μm and kept in refrigerator. Then, the prepared extract was used for the synthesis of CuO NPs and Ag/CuO NCs.

3.2. Preliminary Phytochemicals screening of the *Ocimum lamiifolium* Plant Extract

The presence of alkaloids, flavonoids, phenols, saponins, steroids and tannins (gelatin) in the plant extract were examined according to the literature's [20, 71–73].

3.2.1. Test for phenols

Ferric Chloride Test: 1 mL of plant extract was taken in a test tube, and a few drops of 10% ferric chloride (FeCl_3) was added and the formation of dark green color indicates the presence of Phenols.

3.2.2. Test for alkaloids

Dragendroff's Test: Plant extract (1 mL) was taken in the test tube and a few drops of Dragendroff's reagent (Potassium bismuth iodide solution) was added into it, and orange or orange-red precipitate formation indicates the presence of alkaloids.

3.2.3. Test for saponins

Froth (foam) Test: 1 mL of plant extract was placed in a test tube containing water, shaken well, and noted for a stable foam that persists for at least 2 min.

3.2.4. Test for flavonoids

Sodium hydroxide test: 2 mL of sodium hydroxide was added in 2 mL of aqueous extract. The appearance of yellow color was regarded as the presence of flavonoids.

3.2.5. Test for steroids

Liebermann–Burchard reaction: 2 mL of acetic anhydride and 2 mL conc. H_2SO_4 was added to 2 mL of the extract. The change of color from violet to blue confirms the presence of steroids.

3.3. Synthesis of CuO NPs

Synthesis of CuO NPs capped with *Ocimum lamiifolium* leaf extract was conducted according to the reported literature with slight modifications [22, 74]. 0.97 g of copper (II) nitrate trihydrate ($\text{Cu}(\text{NO}_3)_2 \cdot 3\text{H}_2\text{O}$) was dissolved in 40 mL of deionized water. Meanwhile, 20 mL *Ocimum lamiifolium* plant extract was added to the solution for the reduction of metal ions. The binary mixture of the solution was maintained at 70 °C for 3 h until the color of the mixtures changed from green to brown solution.

After 3 h, the solution was cooled, carefully transferred and centrifuged for 30 min at 2000 rpm and the process was repeated three times. The centrifugate was washed with distilled water followed by absolute ethanol twice. Finally, the precipitate was collected on a watch glass and air-dried, then; the powder was collected for further analysis.

3.4. Synthesis of Ag doped CuO nanocomposites

Synthesis of Ag/CuO nanocomposites using *Ocimum lamiifolium* leaf extract was carried out based on the literature reports [22, 74–76] with slight modifications. 0.97 g of copper (II) nitrate trihydrate ($\text{Cu}(\text{NO}_3)_2 \cdot 3\text{H}_2\text{O}$) solution was prepared in 40 mL of deionized water. After its complete dissolution, 0.032 g of silver nitrate (AgNO_3) was dissolved in 5 mL of deionized water to form 0.0375 M solution of silver nitrate, and added to the copper solution. Then, 20 mL of *Ocimum lamiifolium* plant extract was mixed into the mixture of the solution and the reaction mixture was maintained at 70 °C for 3 h until the color of the mixture changed to brown, which indicates the formation of Ag/CuO NCs. The resultant solution was kept at room temperature, washed with deionized water followed by absolute ethanol by centrifugation, and repeated three times. It was then allowed to air dry on a watch glass to produce its powder which was used for different characterizations. To study the optimum conditions for Ag/CuO NCs synthesis, the experiments were carried out with a different volume of *Ocimum lamiifolium* aqueous extract (10, 20, and 30 mL), pH (5, 7, 9, and 11), copper ion concentration (0.05, 0.1, 0.15 M), silver ion concentration (0.025, 0.0375, and 0.05 M), temperature (30 to 80 °C), and reaction time from (1 to 4 h) within 1 h difference. The pH of the reaction was adjusted using 0.1 M NaOH and 0.1 M HCl. The effect of these parameters on the synthesis of Ag/CuO NCs was monitored by a UV-Vis spectrophotometer.

3.5. Characterizations of the Synthesized CuO NPs and Ag/CuO NCs

The optical properties of synthesized nanoparticles were identified by UV–Vis (Ultraviolet–Visible spectrophotometer, Analytical jena, Germany) and spectral measurements were carried out with in a range of 200–800 nm. Functional groups present or bioactive molecules responsible for the reduction of metal ions present in a sample were identified by FT-IR (65 FTIR Perkin Elmer) and the spectra was recorded between 4000–400 nm. Structure and crystallite size of nanoparticle was obtained by XRD (X-ray diffraction; XPERT-PRO Machine)

an angle range between 30-80° with $\text{CuK}\alpha$ radiation in a θ - 2θ configuration, and morphology of synthesized nanoparticles and nanocomposites was analyzed by SEM (JSM-7900F).

3.6. Application of Synthesized CuO NPs and Ag doped CuO NCs

3.6.1. Photocatalytic activity study

The photocatalytic activity of all the synthesized samples were assessed by the degradation of Methylene Blue dye as a model pollutant (Fig. 7), based on the reported literatures [78, 79] with slight modifications.

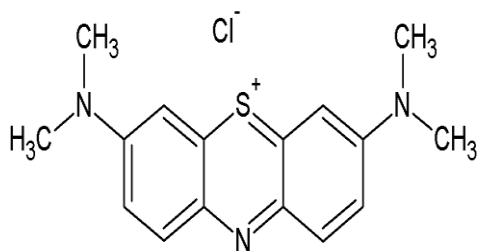


Figure 7: Chemical structure of Methylene blue dye (MB).

Firstly, 1000 mg/L of MB dye solution was prepared as a stock solution. From this stock solution, 10 mg/L was prepared in 100 mL of DI water. 30 mg of Ag/CuO catalysts were added into 100 ml of 10 mg/L of MB solution in a beaker. A mixture of the sample suspension was placed in the dark for 35 min and stirred with a magnetic stirrer to reach an adsorption-desorption equilibrium between MB and the photocatalysts surface. After that, the sample suspensions were exposed to visible light (LED lamp, 200 W) at different time intervals (20, 40, and 60, 80, 100, 120 min) and 5 mL of sample suspensions obtained was withdrawn and centrifuged for five min, and the absorbance of methylene blue in the resultant solution was monitored in the wavelength range of 400-800 nm in a UV-Vis spectrophotometer.

All the above procedures were performed for Methylene blue dye solution without adding the catalyst. Distilled water was used as a reference.

The degradation efficiency (%) was calculated as follows

$$\% \text{ Degradation} = \frac{A_0 - A_t}{A_0} \times 100$$

Where, A_0 is absorbance of dye at initial stage and A_t is at a time “t” [80].

The effect of different parameters like catalyst dosage, contact time, concentration of pollutant, effect of pH, and effect of irradiation time were studied during the degradation of MB dye by Ag/CuO NCs. The catalytic activity of CuO NPs was checked at optimum condition by following all the above procedure and compared with Ag/CuO NCs.

3.6.2. Point of zero-charge analysis (PZC)

The point of zero charge (pH_{zpc}) is the pH at which the total number of positive and negative charges on catalyst surface becomes zero [81]. Point of zero charge analysis was performed according to the procedure conducted in the literature [82]. In a series of 50-mL plastic bottles, 30 mg of Ag/CuO NCs were added with 20.0 mL of 0.1 M NaCl solution. The pH was adjusted with 0.1 M HCl and 0.1 M NaOH as needed to obtain the appropriate pH range of 3, 4, 5, 6, 7, 8, 9, 10, 11 and 12. The pH values of the supernatant in each bottles were denoted as pH_i . The samples were shaken for 24 h using Shaker, at 200 rpm. After 24 h, pH_f values in each bottles were measured and denoted as pH_f . The PZC was obtained from the plot of $\Delta pH = (pH_f - pH_i)$ against pH_i .

3.6.3. Reusability test of the Ag/CuO NCs

The reusability of Ag/CuO NCs was appraised for the degradation of MB dye in the optimized reaction conditions by following the literature's [83, 84]. So, the nanocomposites were gathered from the decolorized solution by centrifugation. The catalyst was washed twice with deionized water to remove any residue from the catalytic reaction mixture. The separated catalyst was air dried and reused again. The percentage degradation of the MB was calculated and compared with the first run.

3.6.4. Antibacterial activity

The synthesized CuO NPs and Ag/CuO NCs were screened for *in-vitro* antibacterial activities against four bacteria strains (*Escherichia-coli*, *Staphylococcus aureus*, *Bacillus cereus*, and *Salmonella typhae*) by Agar disc diffusion method [85–87] at Jimma University, Microbiology laboratory. The bacterial stock cultures were maintained on the nutrient agar slants at 4 °C. Freshly, grown liquid culture of the test strains having similar turbidity with 0.5McFarland were seeded over the Mueller-Hinton agar medium with sterile swab. The disc

measuring 6 mm in diameter was prepared from Whatmann filter paper sterilized by dry heat at 121 °C for 2 h. The different concentrations of CuO NPs, and Ag/CuO NCs (100, 75, 50 and, 25 mg/mL) were prepared by dissolving synthesized nanoparticles in DMSO. Then, sterilized 6 mm filter paper discs were soaked in each NPs and NCs solution. The discs impregnated with the test solutions were placed on a cultured glass plate at equal distance to one another to avoid overlap of zones of growth inhibitions. The growth inhibition zone was measured in mm after 24 hour's incubation at 37 °C and compared with the standard drug (Gentamycin). 1% DMSO was used as a negative control and Gentamycin (10 mg/mL) was used as a standard drug. All the above procedure were repeated three times and mean standard deviation of a zone of inhibition were taken.

4. RESULT AND DISCUSSION

4.1. Preliminary Phytochemical Screening of the *Ocimum lamiifolium* Plant Extract

During this study was conducted Phytochemical tests were performed to identify classes of secondary metabolites present in the leaves of *ocimum lamiifolium* plant extract. The primary Phytochemical screening of the extract showed the existence of flavonoids, tannins, saponins, and alkaloids (Appendix 1).

Table 2: Phyto-chemical components of *ocimum lamiifolium* plant extract

Phytochemicals	Chemical tests	Results
Flavonoids	Sodium hydroxide test	+
Tannin's	Ferric chloride test	++
Steroids	Steroids test	-
Alkaloids	Wagner's test	+
Saponins test	Froth formation test	+

Note: (+) indicates presence of Phytochemicals and (-) indicates absence of Phytochemicals, (++) higher intensity of color formed.

The study showed that the plant extract contains various classes of Phytochemicals such as flavonoids, tannins, alkaloids, and saponins. However, steroids have not been detected in the leaves of plant extract (Table 2, Appendix 1). The higher intensity of color formed on the ferric chloride test indicates that the plant is rich in tannins. Functional groups present in these phytochemicals especially hydroxyl group (OH), and carbonyl (C=O) group act as reducing and stabilizing agents for the synthesis of nanomaterials.

This result is in good agreement with the literature [20] in which it was tested for the presence of phytochemicals in *Ocimum lamiifolium* (Damakese) plant extract. However, according to [20] report alkaloid was not present in the extract but this study revealed that the presence of alkaloids. This may be due to the type of solvent used during extraction, since different solvents

can extract different families of Phytochemicals based on their polarity, hence varying the biological activity of the extracts [88].

4.2. Synthesis of CuO nanoparticles and Ag/CuO nanocomposites

During the synthesis of CuO NPs, the color of the mixtures of leave extract and copper nitrate trihydrate solution was green at the beginning. After heating for 3 h with continuous stirring at 70 °C, brown color was observed which indicates the formation of CuO NPs. Ag/CuO NCs were synthesized in a similar way to CuO NPs but, with the addition of silver dopant and brown color was observed that indicates the formation of Ag/CuO NCs (appendix 2b). The copper and silver ions was reduced to their corresponding CuO NPs and Ag/CuO NCs, and the synthesized nanoparticles and nanocomposites were capped through phytochemicals present in plant extract [21].

4.3. Parameters Optimization for the Synthesis of Ag/CuO NCs

4.3.1. Concentration of $\text{Cu}(\text{NO}_3)_2 \cdot 3\text{H}_2\text{O}$ optimization

In this study, an optimization approach for synthesizing Ag/CuO NCs with small particle size and smaller bandgap were reported. Formation of silver doped copper oxide nanocomposite was studied by the varying copper nitrate trihydrate ($\text{Cu}(\text{NO}_3)_2 \cdot 3\text{H}_2\text{O}$) concentrations from 0.05, 0.1, and 0.150 M, and by keeping plant extract volume (20 mL), concentration of silver (dopant) (0.05 M), reaction time, and temperature constant. To synthesize Ag/CuO NCs at optimum conditions the ratio of the volume of plant extract must correspond to the concentration of copper precursor used [89]. The intensity of the absorption peak was increased due to increasing the concentration of copper nitrate trihydrate ($\text{Cu}(\text{NO}_3)_2 \cdot 3\text{H}_2\text{O}$) solution from 0.05 to 0.1 M (Appendix 3). This may be due to the formation of more Ag/CuO NCs as the reaction progresses since the intensity of the surface Plasmon peak has direct proportionality with the density of synthesized nanoparticles in the solution [90]. By further increasing the concentration of copper nitrate trihydrate to 0.15 M intensity become decreased, and the absorption peak becomes broader because of the deficiency of molecules of leaf extract to act as capping agents and which may cause aggregation of nanoparticles [90, 91]. The result obtained was in close agreement with a recent report [91] in which the effect of the concentration of AgNO_3 on the green synthesis of silver nanoparticles was studied. Therefore, 0.1 M copper nitrate trihydrate solution was taken as the optimum condition to biosynthesize Ag/CuO NCs.

4.3.2. Plant extract optimization

The synthesis of Ag/CuO NCs using plant extract is mainly influenced by the types of biomolecules found in plant extracts and the volume used. The volume of plant extracts used in the synthesis of nanomaterials plays a significant role in the reduction of metal ions to reduced metal [9]. To get the optimum amount of leaf extract for the reduction of Ag⁺ and Cu²⁺ ion, the volume optimization of *Ocimum lamiifolium* leaf extract was studied.

(Appendix 4) shows the UV-Vis spectra for Ag/CuO NCs formation after 3 h reaction time using a fixed Cu(NO₃)₂·3H₂O concentration (0.1 M) and AgNO₃ concentration solution with different volumes of *Ocimum lamiifolium* leaf extract. A redshift in the wavelength from λ_{\max} 377 nm to 390 nm was observed when the volume of extract was increased from 10 to 20 mL and the peak formed was narrow. The narrow peak formed indicates, a greater amount of plant extract would increase the nucleation rate and lead to the generation of smaller Ag/CuO NCs in the solution [83]. This is attributed to the Phytochemicals present in the plant extract, which are responsible for the bioreduction and stabilization of the NPs [92].

However, by increasing plant extract further to 30 mL broader absorption peak was observed. This resulted in an increase in particle size, because of the fast reduction of Cu and Ag ions that facilitates further growth of nanocomposite through a phenomenon called Ostwald ripening, and broadness of the peak may be due to agglomeration of nanocomposite [90, 93]. Therefore, 20 mL of plant extract was taken as the optimum condition to bio-synthesize Ag/CuO NCs in this study. The result obtained was in close agreement with the literature's [77] in which the effect of volume of plant extract on the green synthesis of CuO NPs was studied.

4.3.3. Concentration of dopant optimization

The absorption peak of Ag/CuO NCs was also affected by the concentration of dopant [94]. To see the effect of concentration of dopant (Ag) on the absorption peak of CuO NPs; the dopant concentrations were varied as (0.025 M, 0.0375 M, and 0.05 M) while other parameters were kept constant. Redshift was observed in the wavelength range from 376 to 419 nm while the concentration of dopant was increased from 0.025 to 0.0375 M and while it was increased to 0.05 M, the absorption peak was decreased to 392 nm (Appendix 5) which resulted in a change

in the optical band gap value. This result reveals that the bandgap of Ag/CuO nanocomposites increases with an increasing concentration of Ag⁺ ions greater than 0.0375 M.

A similar result was reported by literature [95] that studied the effect of concentration of Mn dopant on surface Plasmon resonance peak of ZnO nanoparticles and energy bandgap. According to literature [95] report, as the concentration of Mn (dopant) increases more, blue-shift was observed which results in an increased bandgap.

4.3.4. Effect of pH

The pH is one of the factors that influence the size, shape, and composition of nanoparticles and nanocomposites [96]. The pH in aqueous media can highly influence the progress of the metal ion reduction reaction [97]. The role of pH on nanomaterial synthesis could be seen in its effect on the capping and stabilizing abilities, and subsequently the growth of the nanoparticles. The presence of OH⁻ ion in an alkaline pH environment might enhance the reducing and stabilizing capabilities of the biomolecules in the leaf extract due to the better accessibility of functional group present in extract for nucleation at alkaline pH [98].

Green synthesis of silver-doped copper oxide nanocomposites using aqueous extract of *Ocimum lamiifolium* leaves was examined over a pH range from 5 to 11. As shown in (Appendix 6), the synthesis of Ag/CuO NCs using 20 mL leaf extract and 40 mL of 0.1 M Cu(NO₃)₂·3H₂O was carried out at different pH values, namely pH 5, 7, 9, and 11. Without performing any pH modification, after mixing the leaf extract and Cu(NO₃)₂·3H₂O solution, the pH value of about 5.1 was recorded. At this acidic pH, a broader absorption peak was observed. As the pH was increased from pH 7 to pH 9, a redshift (from 437 nm to 473 nm) was observed in the SPR peak (Appendix 6). This redshift mostly enhances the nanocomposite size; since a highly broad spectrum was formed especially at pH 9 [99]. By further increasing to pH 11, blue shift was observed at λ_{\max} 452 nm that could be attributed to the decrease in the particle size. Therefore, pH 11 was taken as an optimum condition to bio-synthesize Ag/CuO NCs.

The result obtained was in a match with the findings reported in the literature [83, 100] that CuO NPs were synthesized at optimum pH of 11. Therefore, the result obtained shows that in acidic

pH, nanocomposites become aggregated rather than forming nucleation, while at alkaline pH, great numbers of nuclei formed instead of aggregation [101].

4.3.5. Effect of temperature

Temperature is one of the major factors that significantly influence the shape, size, stability, and yield of the nanocomposites synthesized via a green route. In most cases, the synthesis of nanoparticles using green technology requires temperatures less than 100 °C or ambient temperature [41]. The effect of temperature on the green synthesis of Ag/CuO NCs was studied by varying it from 30 to 80 °C by keeping all the other factors constant (Appendix 7).

At 30 and 40 °C, the Ag/CuO NCs did not present any absorption peaks indicating that no Ag/CuO NCs were formed [102]. As the temperature increased from 50 to 70 °C the intensity of the peak increased and especially at 70 °C a narrow peak was formed. This may be related to increasing reaction temperature improves the reaction rate and high-temperature increases the nucleation rate. By further increasing temperature to 80 °C the absorption peak becomes broader which may lead to an increase in particle size [103]. Therefore, 70 °C was taken as an optimum condition to synthesize Ag/CuO NCs.

4.3.6. Effect of reaction time

Reaction time is essential for the synthesis and stability of nanoparticles and nanocomposites [104]. The effect of reaction time was studied during the green synthesis of silver-doped copper oxide nanocomposites. The effect of reaction time was conducted by analyzing samples through the UV-vis spectrum by every 1 h for 4 h (Appendix 8). The UV-Vis analysis of the samples displayed a small intensity peak at 1 h, and the intensity of the band increased, and the peak become narrowed as time progressed to 3 h. This indicated enhanced nucleation rate, and formation of small-sized NCs. Nevertheless, after 3 h the absorption peaks formed were identified to be considerably similar.

Therefore, the literature [105] found a similar result to this finding and concluded that increasing the reaction time increases the rate of reduction of metal ions until the reaction reaches completion. But according to the literature [106, 107] as contact time increases the overall concentration of the nanomaterial increases until an equilibrium is reached and a longer reaction

time may cause an increase in the size and also enhance the agglomeration of the NCs rather than nuclei formation.

4.4. Characterization of Synthesized CuO Nanoparticles and Ag/CuO Nanocomposites

4.4.1. UV-Vis spectroscopy Analysis

During analysis of synthesized nanomaterials by UV-Vis spectroscopy, the absorption peak appeared at 308 and 452 nm confirms the formation of CuO NPs, and Ag/CuO NCs respectively (Fig. 8 (a and b)). The result obtained was closely matched with the recent reports [23] in which Ag/CuO NCs was synthesized from *Muntingia Calabura* leaf extract and the maximum absorption peak was obtained at 450 nm, whereas absorption peak of CuO NPs was obtained at 305 nm [12].

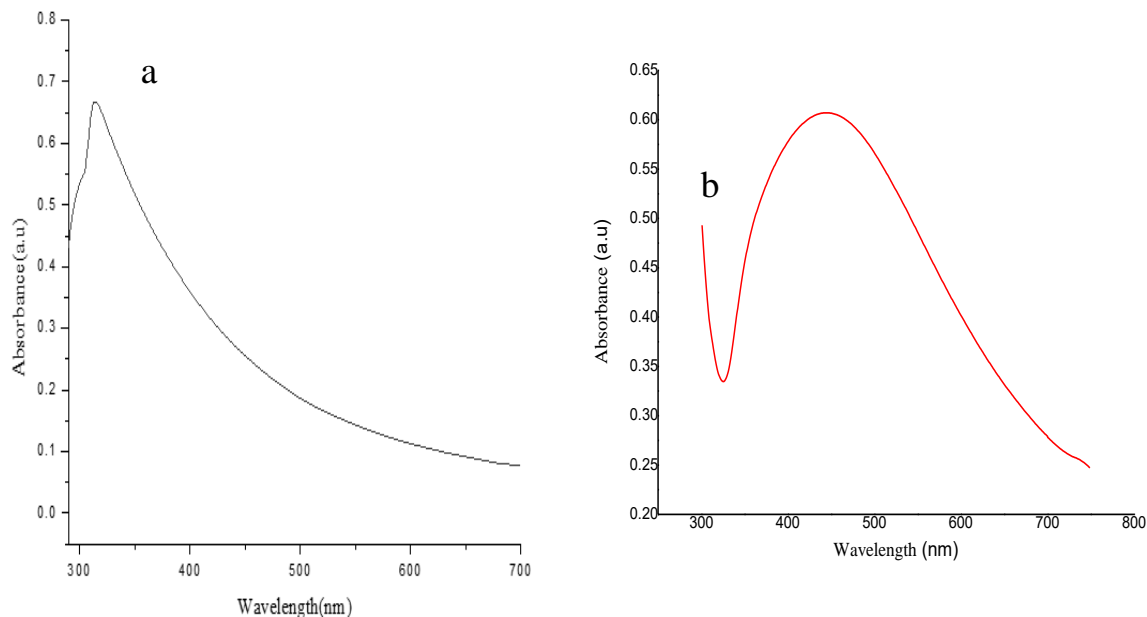


Figure 8: UV-Vis spectra of (a) CuO NPs (b) Ag/CuO NCs

The UV-Vis absorption spectra of Ag/CuO NCs were broad compared to CuO NPs peak; this may be because of the wide size distribution of the synthesized nanocomposite. In addition to this, the UV-Vis spectra of green synthesized CuO NPs were narrow this indicates the formation of smaller sized CuO NPs [103].

The energy band gap of CuO NPs and Ag/CuO NCs were depicted in (Fig. 9 (a and b)). It was determined using the tauc relation. Tauc plot is a convenient way of studying the optical

absorption spectrum of a material. According to the tauc relation, the absorption coefficient α for direct bandgap material is given by, $\alpha h\nu = A(h\nu - E_g)^m$. Where A is the optical constant, α is the absorption coefficient, E_g is the optical band gap and m is an index, which assumes the values 1/2, 3/2, 2, and 3 depending on the nature of electronic transition responsible for the reflection. It has the photon energy ($h\nu$) on the X-axis and a quantity $(\alpha h\nu)^2$ on the Y-axis and extrapolating the linear portion of the curve to the X-axis yields the bandgap energy of the material [61].

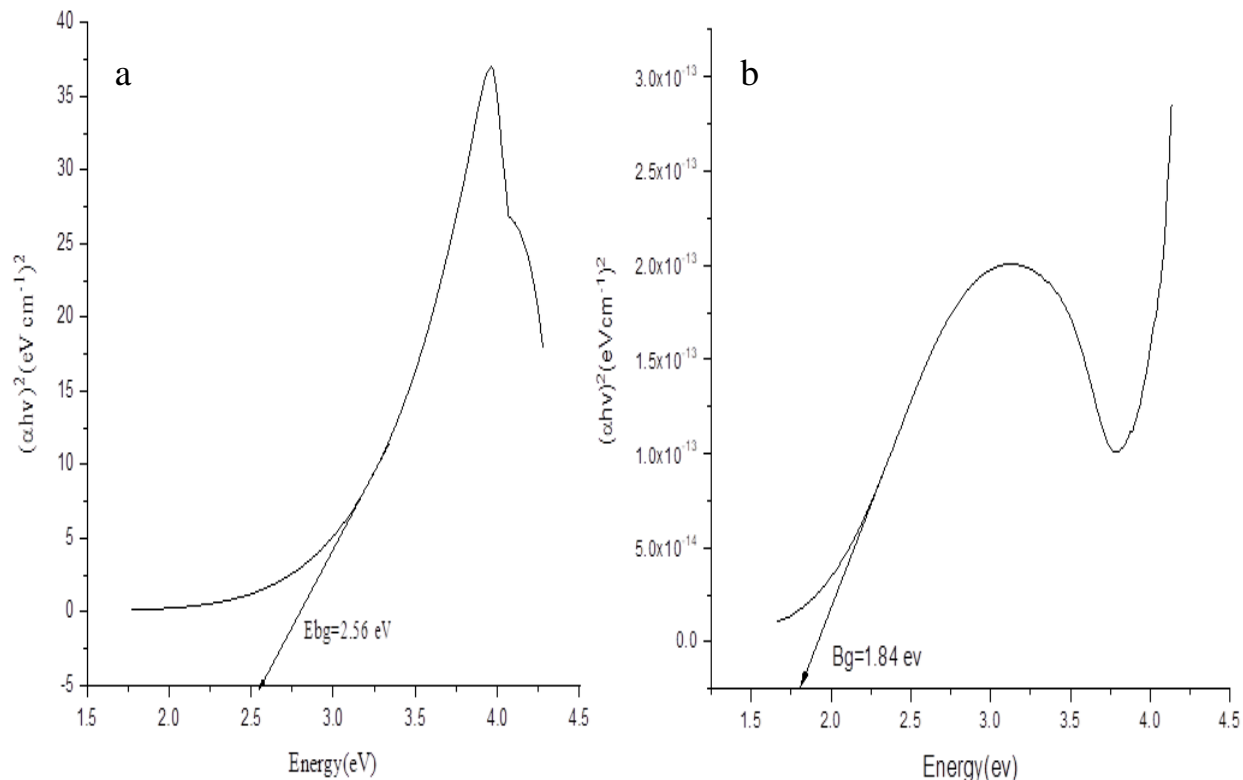


Figure 9: The tauc plot of (a) CuO NPs (b) Ag/CuO NCs

From (Fig. 9 (a and b)), the energy band gap of green synthesized CuO NPs and Ag/CuO NCs were 2.56 and 1.84 eV respectively. Generally, the energy band-gap of green synthesized CuO NPs was decreased by doping Ag to CuO NPs that mainly indicates improved conductance because of doping [77]. Depending on works of literature [23, 77, 108], the characteristic energy bandgap of CuO NPs has been reported to be between 1.8 eV and 2.5 eV, which is in close agreement with present findings.

4.4.2. FT-IR Analysis

The FT-IR spectra were used to confirm the presence of functional group and plant metabolites, which are used for the reduction and stabilization of the green synthesized copper oxide nanoparticles and silver-doped copper oxide nanocomposites. The FT-IR spectra of the synthesized Copper oxide NPs (Fig. 10) depict a broadband absorption peak at 3430 cm^{-1} indicates the stretching of O–H groups in water, and phenols [109].

However, after doping with Ag dramatic reduction in intensity occurred and, this broadband disappeared. This may be related to reduced water content in the Ag/CuO NCs or interaction of the silver with the hydrogen-bonded O–H groups [110]. Characteristic peaks of CuO NPs at 2931 cm^{-1} that shifted to 2923 cm^{-1} in Ag/CuO NCs represent C–H stretching of alkyl group [111]. These C–H stretching and O–H functional groups are adapted from flavonoids and Phenols [22]. A broader band at 2357 cm^{-1} corresponding to strong O = C = O stretch of carbon dioxide. The same band at 2347 cm^{-1} in the doped nanoparticles is much reduced in its intensity. Such differences in reduction in peak intensities can be attributed to differences in reduction mechanism and capping of two specimens in the presence of leaf extract [23].

The Intense peak formed at 1606 cm^{-1} in the spectrum of CuO NPs and the less intense peak formed at 1602 cm^{-1} in the Ag/CuO NCs spectrum is ascribed to C=O (carbonyl). These carbonyl groups indicate the presence of flavonoids, which act as reducing and stabilizing agents for the synthesis of nanoparticles [12]. The peak at 1011 and 1062 cm^{-1} are ascribed to the C-O stretching vibration of O-H groups [12]. The low-intensity band observed around 1414 cm^{-1} occurred in CuO NPs which is shifted to 1396 cm^{-1} after doping by silver may be due to O-H bending vibrations [44, 112]. Peak formed at 823 and 788 cm^{-1} for CuO and Ag/CuO NCs respectively were assigned to the aromatic bending vibration of the C–H group [113].

On comparing the two different spectrums, it is evident that the undoped CuO NPs exhibited sharp absorption bands between 400 and 700 cm^{-1} , while the doped copper oxide nanocomposites exhibited less intense bands in this region. The peak occurred between 400 - 700 cm^{-1} specifically 428 and 514 cm^{-1} for CuO NPs and at 557 cm^{-1} due to silver-doping represent the vibrational modes of Cu-O [44].

FT-IR of plant extract shows only a small variation from synthesized nanoparticles (Fig. 10a). The C=O band noticed in plant extract around 1618 cm^{-1} showed weaker band and shifted to 1606 and 1602 cm^{-1} , and the OH band around 3443 cm^{-1} shifted to 3430 and 3424 cm^{-1} in CuO NPs and Ag/CuO NCs showing stabilization through the carbonyl and OH group of the biomolecules. Therefore, the results confirmed that these biomolecules have efficient reducing and stabilizing capabilities [114]. This result is in agreement with a recent report [22].

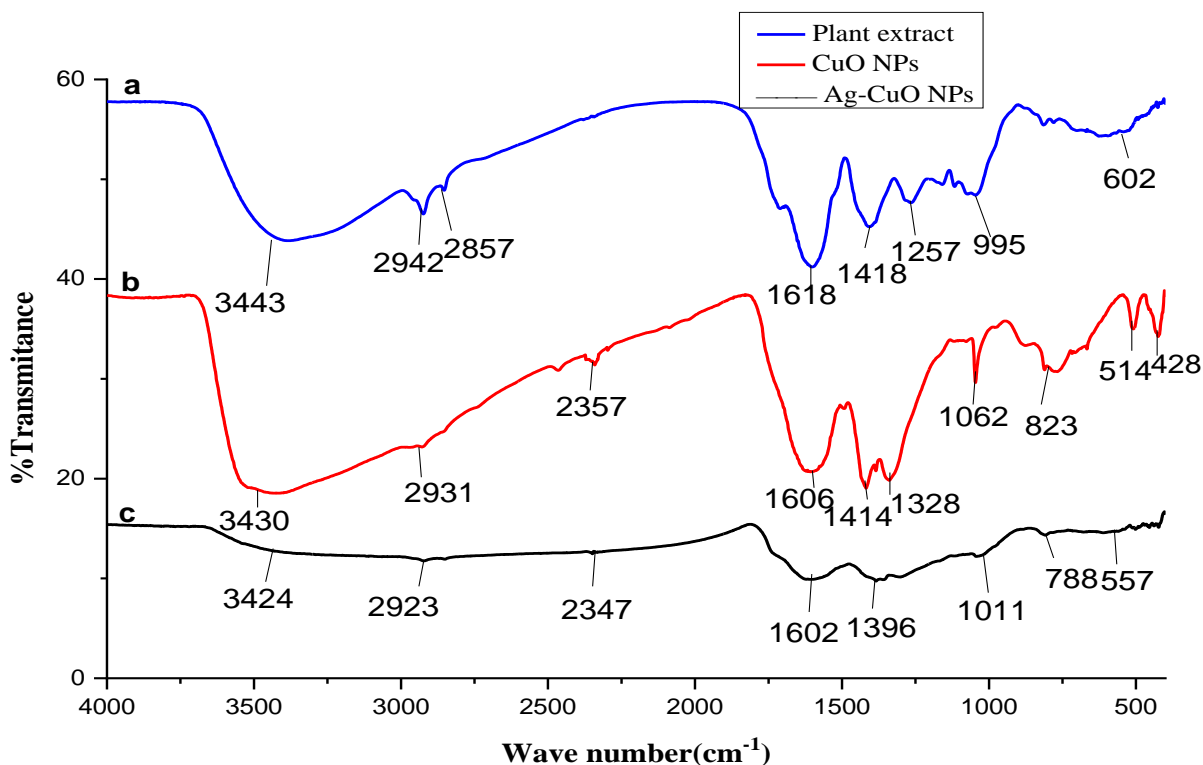


Figure 10: FT-IR spectra of (a) Plant extract (b) CuO NPs (c) Ag/CuO NCs

4.4.3. X-Ray Diffraction Analysis

X-ray diffraction study was carried out on the prepared CuO NPs & Ag/CuO NCs. The crystalline nature of nanoparticles and nanocomposites was confirmed by the powder X-ray diffraction study and diffraction peaks are indexed in (Fig. 11). The diffraction peaks of CuO NPs is at $2\theta = 32.47^\circ, 35.47^\circ, 38.60^\circ, 48.89^\circ, 53.48^\circ, 58.42^\circ, 61.49^\circ, 66.26^\circ, 68.06^\circ, 72.59^\circ$ and 75.20° corresponding to diffraction planes at (110),(-111),(111),(-202),(020),(202),(-113), (-311),(220), (311), and (004) respectively. This result is a well matching with (JCPDS No. 05-

0661) that, the synthesized CuO NPs have a monoclinic phase [115]. After doping CuO NPs with Ag, the formation of four extra peaks were observed in the XRD spectrum of Ag/CuO NCs at $2\theta = 38.65^\circ$, 44.10° , 64.54° , and 77.46° that related to the crystal planes (111), (200), (220), and (311) respectively. These additional four peaks observed were peaks due to silver, and showed face centered cubic silver crystal (JCPDS No. 4- 0783) [116].

In the XRD spectrum of Ag/CuO NCs, Ag represent a significant peak without causing defects on the peak of Cu. This indicates that peak due to impurities does not present in the synthesized nanoparticles. Literature [75] supports this finding. In the diffraction spectrum of Ag/CuO NCs, the peak due to silver is weak due to the low concentration of silver used in the nanocomposite [117, 118]. As shown in the XRD spectra, the intensity of XRD peaks of CuO NPs was relatively decreased when Ag was doped to it. This decrease in intensity of the XRD peak indicates the reduction of crystallinity [106].

The average crystallite size of Ag/CuO NCs and CuO NPs were calculated from full width at half-maximum (FWHM) using Scherrer equation according to the following formula [119].

$$D = \frac{0.9\lambda}{\beta \cos\theta}$$

Where D is the crystallite size (nm), λ is the diffraction wavelength (0.154056 nm for CuK α radiation), θ is the diffraction angle (degree), and β is the full width at half maximum (FWHM) for the diffraction peak (radian). The crystallite size of Ag/CuO NCs, and CuO NPs prepared by using *ocimum lamiifolium* leaf extract were 38.2 nm and 29.1 nm respectively. This result is in close agreement with the literature [76] that reported crystal size of Ag/CuO NCs were between 30-50 nm in range.

However, the size obtained for Ag/CuO NCs in this study is slightly smaller than the result reported by literature [44]. This may be due to the difference in plant extract used during nanocomposite synthesis since plant extract used during the synthesis of nanoparticles and nanocomposites can affect the size of the particles [44]. The size obtained for CuO NPs which is 29.1 nm is in match with recent findings [120] that reported the size of bio-synthesized CuO NPs

28 nm. The crystallite size of CuO NPs was increased by doping of Ag to it. This is due to the large ionic radius of Ag (0.129 nm) [121] compared with Cu (0.087 nm).

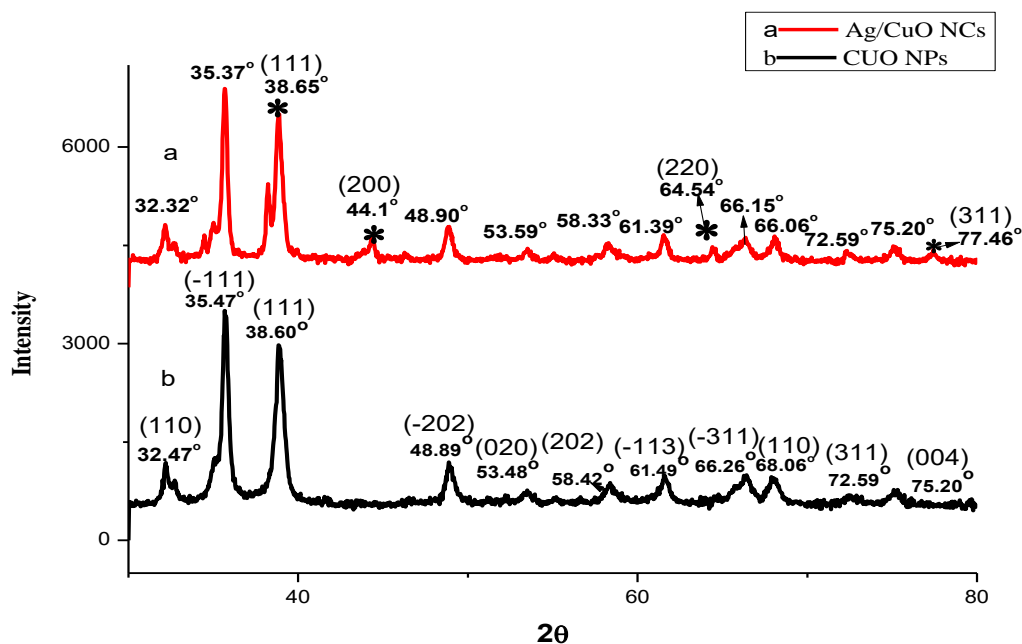


Figure 11: XRD spectra of CuO NPs and Ag/CuO NCs

4.4.4. Scanning Electron Microscopy (SEM) analysis

Fig.12 (a and b) shows the SEM images of the prepared nanoparticles and nanocomposites respectively. The image indicates that the CuO NPs show most of synthesized nanoparticles are and spherical in shape (Fig. 12a). This result is in close relationship with recent findings [109, 113] literature that reported spherical CuO NPs. In case of CuO NPs doped with Ag (Fig. 12b), a mixture of spherical-shaped and rod-like structures was observed. The SEM images of synthesized CuO NPs and Ag/CuO NCs showed a rough surface that may be due to the encapsulation of plant extracts [44].

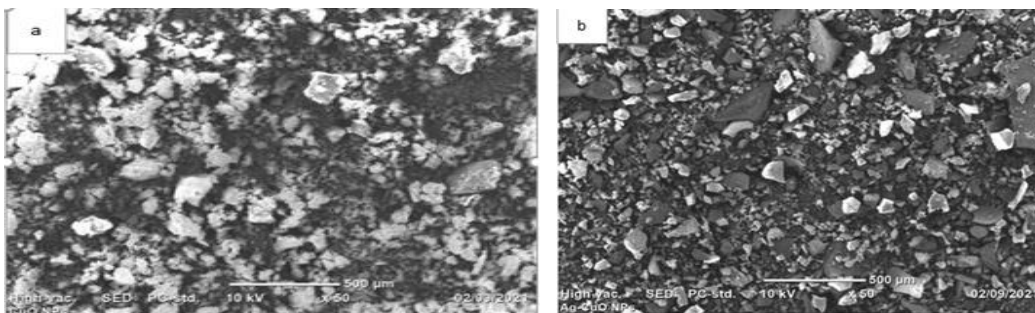


Figure 12: SEM image of (a) CuO NPs (b) Ag/CuO NCs

4.5. Application of synthesized CuO NPs and Ag/CuO NCs

4.5.1. Photocatalytic activity of Ag/CuO NCs

Photocatalytic activity of Ag/CuO NCs was conducted on Methylene blue (MB) dye degradation. Effect of parameters that influences photocatalytic degradation like catalyst dosage, pH, irradiation time, and effect of pollutant concentration was studied under visible light (LED lamp, 200 W) and degradation efficiency of Ag/CuO NCs was compared with that of CuO nanocatalyst at optimum condition. Lastly, the efficiency of sunlight was compared with LED lamps toward degradation of MB at optimum conditions.

4.5.2. Optimization of parameters for the photocatalytic degradation of MB

4.5.2.1. Catalyst dosage

The number of organic pollutants adsorbed on the NPs surface is a crucial factor that influences their photocatalytic performance. Equilibration in the dark is required because it is assumed that photocatalytic reactions of organic pollutants occur in the adsorbed phase [122]. As shown in (Fig. 13a) dark equilibration was performed at 35 min. As it is seen in (Fig. 13b) with an increase in Ag/CuO nanocatalyst from 20 to 30 mg, the degradation percentage was increased from 78 to 83%. Because enhancing catalyst dosage resulted in enhancing the degradation of MB dye by enhancing the active reaction sites of nanocatalyst, and reactive radicals that resulted in enhanced photo-degradation efficiency [123]. By further increasing catalyst dosage to 40 and 50 mg, the percentage degradation of MB becomes decreased slowly due to the enhancement of light reflectance by the catalyst owing to weaker penetration of light [124, 125].

Additionally, as the contact time was increased from 20 to 120 min percentage degradation of MB increased. But, by further increasing to 140 min, negligible change was observed on the

degradation percentage of MB by Ag/CuO NCs. Therefore 30 mg Ag/CuO NCs catalyst and 120 min were taken as optimum condition to study the effect of different parameters on the photocatalytic activity of MB dye by Ag/CuO nanocatalyst.

Similar results were reported by recent literature [126, 127] that with an excess amount of photocatalysts, degradation percentage decreased and this decrease in degradation percentage at high catalyst load is due to weaker penetration of light that resulted in a decrease in the rate of degradation. The effect of catalyst dosage and the effect of contact time on the degradation of MB dye has been graphically represented in (Fig. 13b).

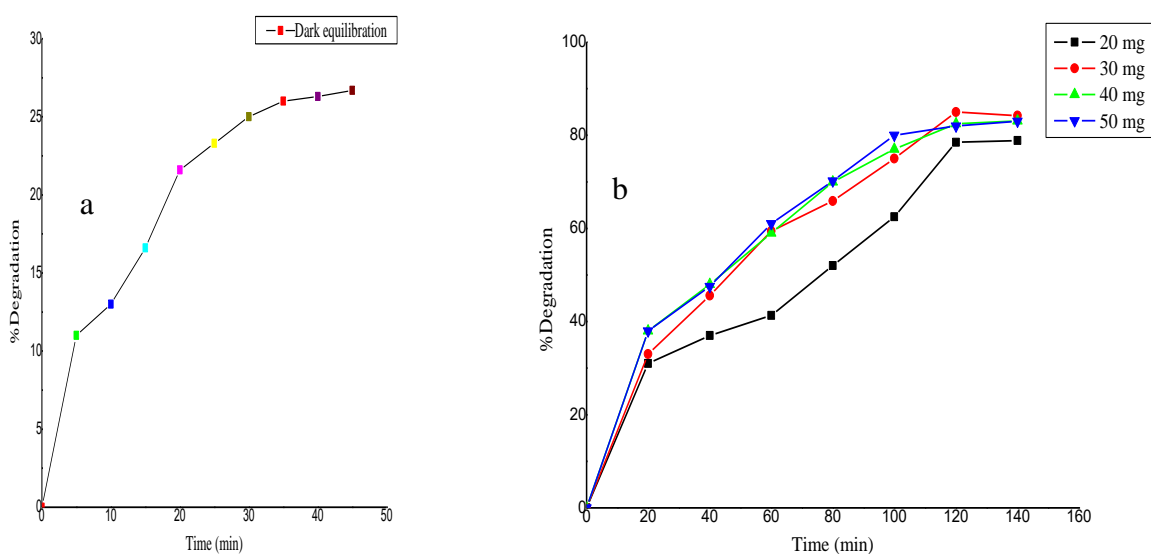


Figure 13: (a) Dark absorption-desorption equilibration (b) Effect of catalyst dosage and contact time on the degradation of MB dye [MB=10 mg/mL, Ag/CuO NCs (20-50 mg)].

4.5.2.2. Effect of pH

Determining the point of zero charge (pHPZC) is substantial to predict the charge on the NPs surface during the photocatalytic degradation process. Since the photocatalysis occurs on the NPs surface, and the performance of the photocatalyst is greatly influenced by the solution pH, the pollutant type and the surface ability to adsorb the pollutant [128]. For the investigation of the point of zero charges of Ag/CuO NCs, the values of the initial and change in pH were plotted. The values of pHPZC of Ag/CuO NCs were determined from the points where the initial

pH equals the final pH. From the (Fig. 14) pHPZC of Ag-CuO NCs was 6.53. Therefore, above pH value of 6.53 surface of Ag/CuO NCs has a negative charge and below this pH, it has a positive charge [129].

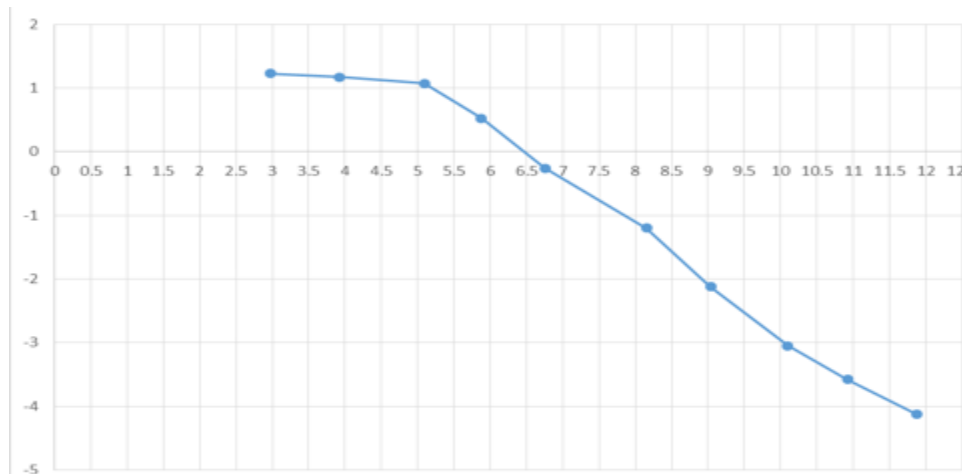


Figure 14: Surface charge of Ag/CuO NPS

Similar result was reported by the literature[109] that surface charge of CuO NPs and Ag/CuO NCs showed negative and close values for pH >6 as they characterize surface charge of Ag/CuO NCs and CuO NPs from zeta-potential.

Adsorption of MB onto the surface of the Ag/CuO NCs was evaluated after 35 min stirring of solution in the dark at different pH values of 6, 7, 8, 9, and 10. The pH of the methylene blue solution was adjusted by adding HCl or NaOH (0.1 M). At 120 min, the degradation percentages of MB by Ag/CuO NCs were 80, 83.5, 85.5, 88.5, and 86% for Ag/CuO NCs prepared at pH values of 6, 7, 8, 9, and 10 respectively. From the result obtained (Fig. 15), the degradation efficiency was increased until pH 9 but after pH 9, it was slowly reduced because it is assumed that as pH increases, the concentration of OH⁻ ions also increases. Consequently, the oxidation reaction rate which leads to hydroxyl radical production will increase and the dye degradation occurs at a higher rate. However, it is notable that as pH increase more and more, there is an increase in repulsive forces between the photocatalyst charged surface with negative potential and OH⁻ ions. This resulted in a decrease in dye adsorption rate and hydroxyl radical generation that play significant role for the degradation of dyes [130].

Similar results were reported by literature [131] in which, as the pH of the solution increases more and more the degradation efficiency decreases because of an increase in repulsive forces between negatively charged photocatalyst surface and hydroxide ions. This study confirmed that the MB showed more degradation in the alkaline condition specifically at pH 9 and this was due to the adsorption of more concentration of MB dyes on Ag/CuO NCs surface [132].

Generally, in the acidic medium (pH 6) the surface of the catalysts is positively charged, as a result, there was repulsive force between photocatalyst surface and cationic MB which hinder higher binding between the two surfaces hence decreased photodegradation. When the pH of the dye solution became more basic (pH 9), the surface tends to acquire a negative charge thereby resulting in increased adsorption of dyes because of the rising electrostatic attraction between cationic MB dye and the negatively charged Ag/CuO NCs catalyst surface, and enhances degradation percentage. This finding is in agreement with previously reported results [133, 134].

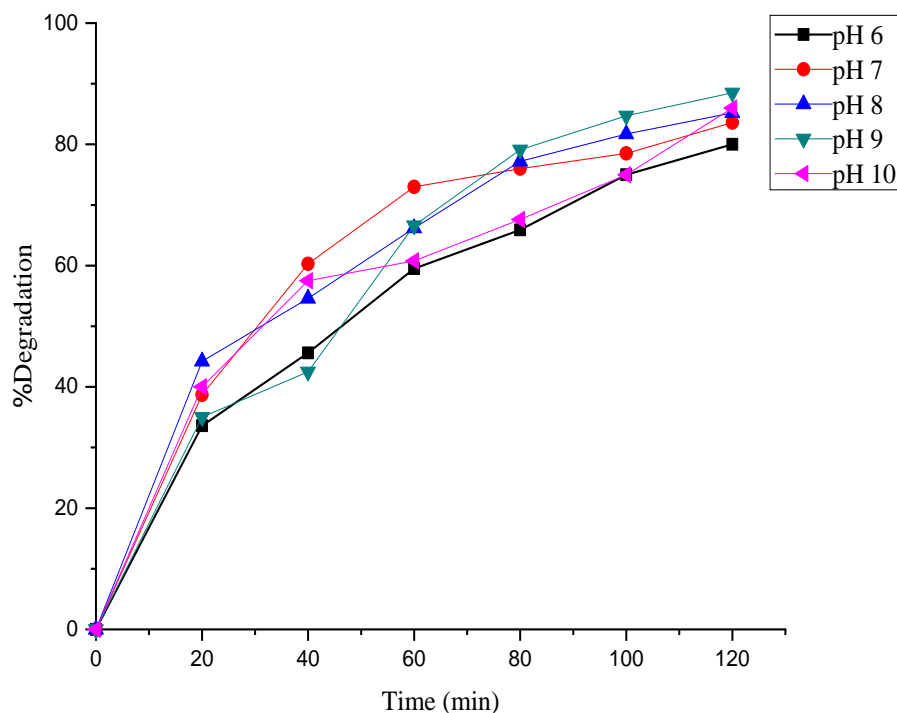


Figure 15: Effect of pH on the degradation of MB dye (MB=10 mg/mL at 120 min)

4.5.2.3. Effect the irradiation time on the MB dye degradation

UV–Vis absorbance spectra were investigated to show the impact of irradiation time on the degradation of MB dye and degradation percentage was calculated by measuring absorbance. The intensity of absorbance peak was highly reduced using Ag/CuO NCs than CuO NPs, and 88.5 and 76.2% of MB dye was degraded by Ag/CuO NCs and CuO NPs respectively (Fig. 16a and b). The result obtained was slightly lower than [44].

This may be due to different light sources used, since literature [44] used Xe lamp as an excitation source. The better catalytic performance of Ag/CuO NCs than CuO NPs could be due to reduction in the electron-hole recombination's [127]. According to the literatures [135, 136], 75 and 78% of MB were degraded by green-synthesized CuO NPs which is in close agreement with this finding. The decrease in absorbance intensity at 665 nm with increasing irradiation time is indicated in (Figures 16, 17, and 18) below. This decrease in absorbance intensity indicates the degradation (decrease in concentration) of MB.

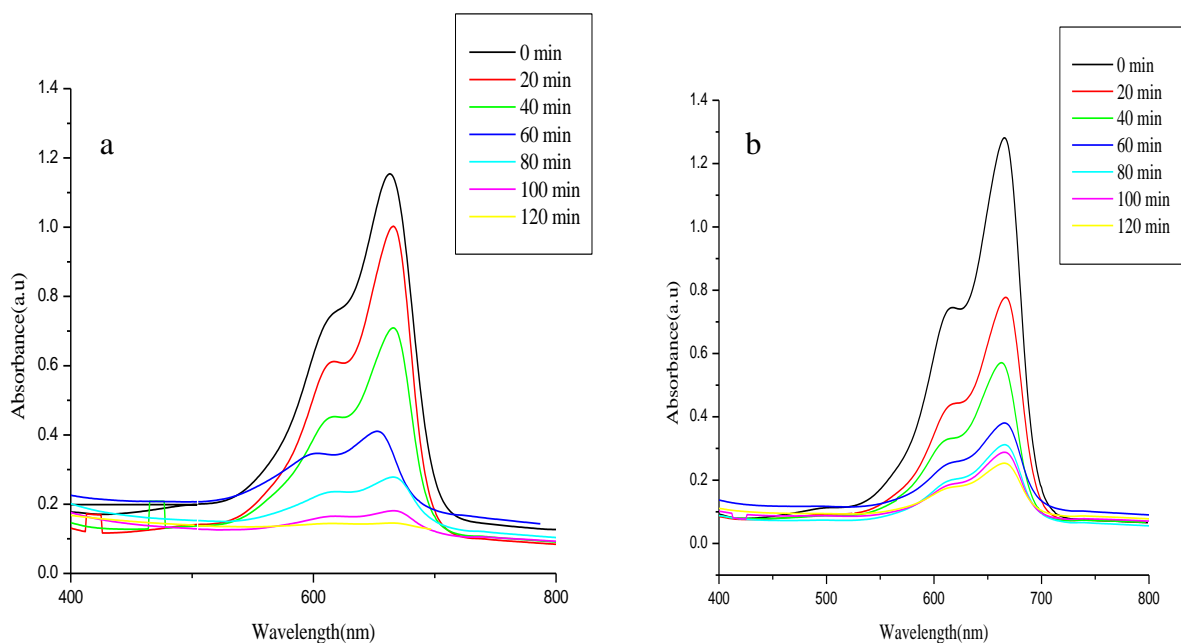


Figure 16: Effect of irradiation time on the degradation of MB using (a) Ag/CuO NCs and (b) CuO NPs at different time interval, (MB=10 mg/L, pH 9) under LED lamp, 200 W irradiation.

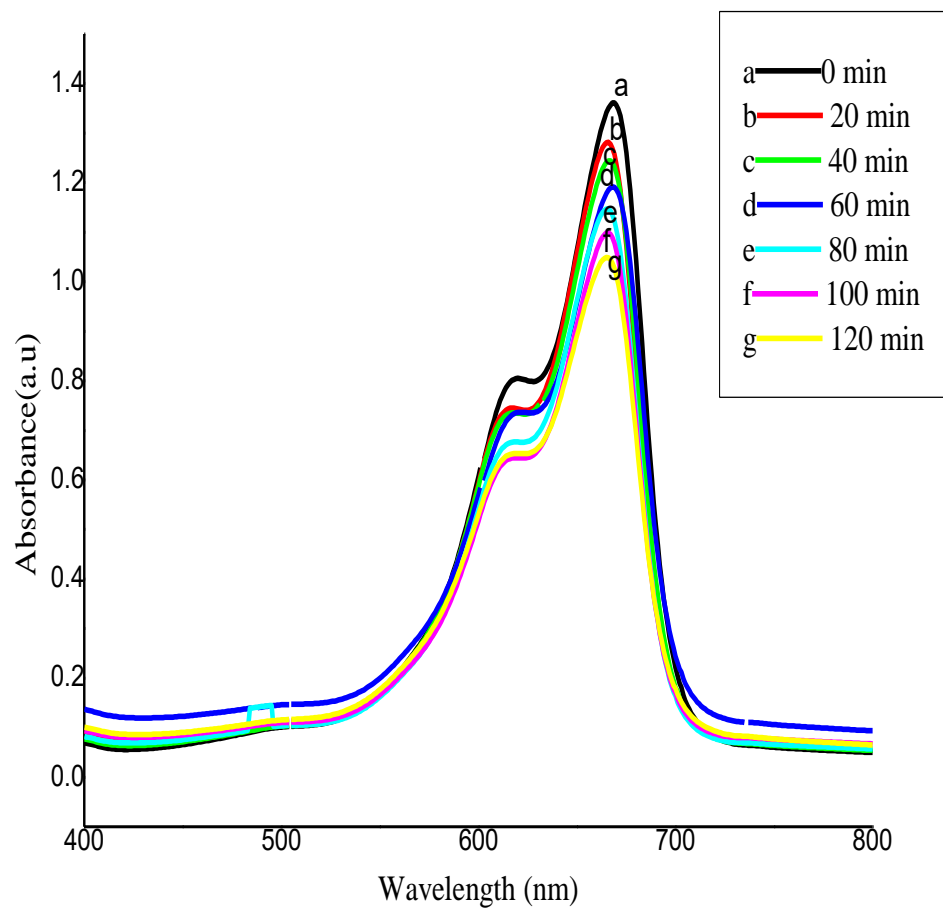


Figure 17: Effect of irradiation time on the degradation of MB dye without catalyst

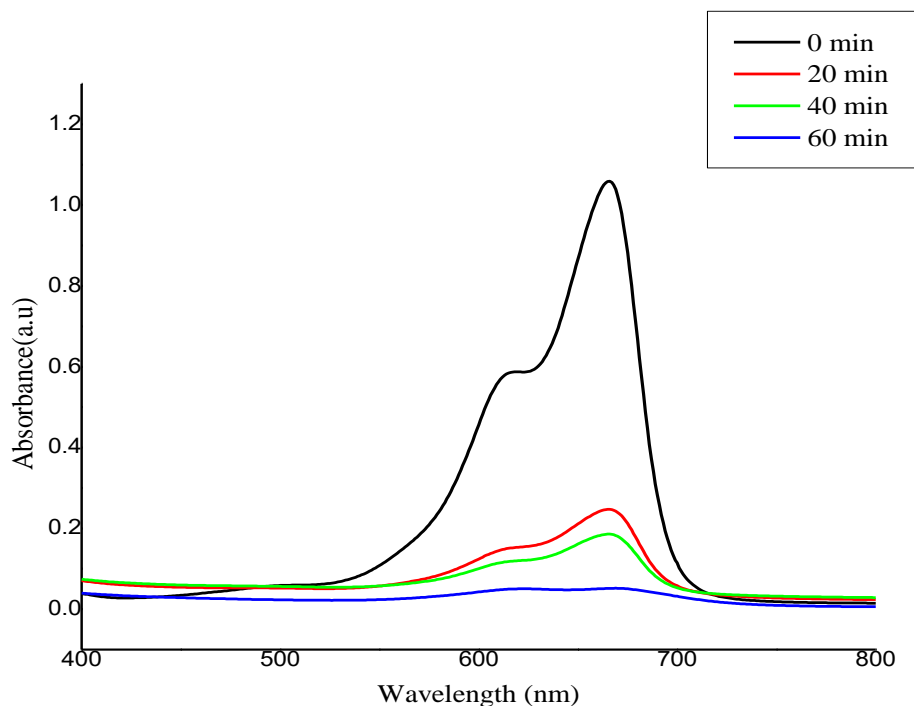


Figure 18: Effect of irradiation time on the degradation of MB dye (30 mg Ag/CuO NCs, MB=10 mg/L, pH 9) by Ag/CuO NCs at different time intervals under sunlight irradiation.

On the other hand, a control experiment was conducted in which MB dye was irradiated with an LED light lamp (200 W) in the absence of the Ag/CuO NCs catalyst (Fig. 17). The findings showed that no major change in the intensity of absorption peak was observed and only 27.2% of the dye was degraded without catalyst. This indicated that the direct photolysis of MB dye was not much effective in the absence of nanocatalyst. A Close result was observed by literature [137] and only 30% of MB dye was degraded without the addition of ZnO catalyst. However little variation in degradation percentage between this finding and their report may be due to difference in irradiation source; since they used UV-light source.

For comparison of degradation efficiency of Ag/CuO NCs under LED light lamps and sunlight as seen from (Fig. 16a and 18), the intensity of absorption peak was reduced rapidly within 60 min of irradiation time by using sunlight as an irradiation sources. This indicated that the degradation of MB in sunlight is faster than LED lamps, because LED lamps had weak UV

intensity compared with the sunlight; it took more time for them to help the photocatalytic degradation of the dye [138].

Hence, the degradation efficiency for the system under LED lamps showed a lower rate, which finally resulted in 88.5% degradation after 120 minutes, while 95.1% of MB dye was degraded within 60 min. This finding is in close agreement with recent reports [138, 139] and revealed that sunlight degradation is faster and more efficient than LED lamp sources, fluorescent lamps, etc. Generally, at 120 min color of MB dye was disappeared (Appendix 9).

4.5.2.4. Effect of initial MB dye concentration

The concentration of dye is one of the main parameters that was changed the degradation efficiency in photocatalytic degradation [140]. The effect of the initial dye concentrations on the decolorization of MB was studied under visible light (200W, LED lamp) irradiation by varying the initial MB dye concentration from 10 to 30 mg/L in the presence of 30 mg of Ag/CuO NCs and optimum pH 9. As shown in (Fig. 19), the degradation percentage of MB decreases from 88.5% to 69% when the initial dye concentration reaches from 10 to 30 mg/L respectively. Similar results were reported by literature [84, 134] that increasing the dye concentration cause the dye molecules to absorb light and the photons never reached the Ag/CuO surface, and at high dye concentrations more active sites may be covered with dye ions.

This may lead to the decrease in the production of OH radicals on the surface of the catalyst which plays a significant role in the dye degradation and finally it causes reduced efficiency of dye removal [126, 129]. Thus, the photo-degradation of MB was found better at low concentrations. The concentration of dye effect on decolorization of MB dye has been graphically represented in (Fig. 19) below.

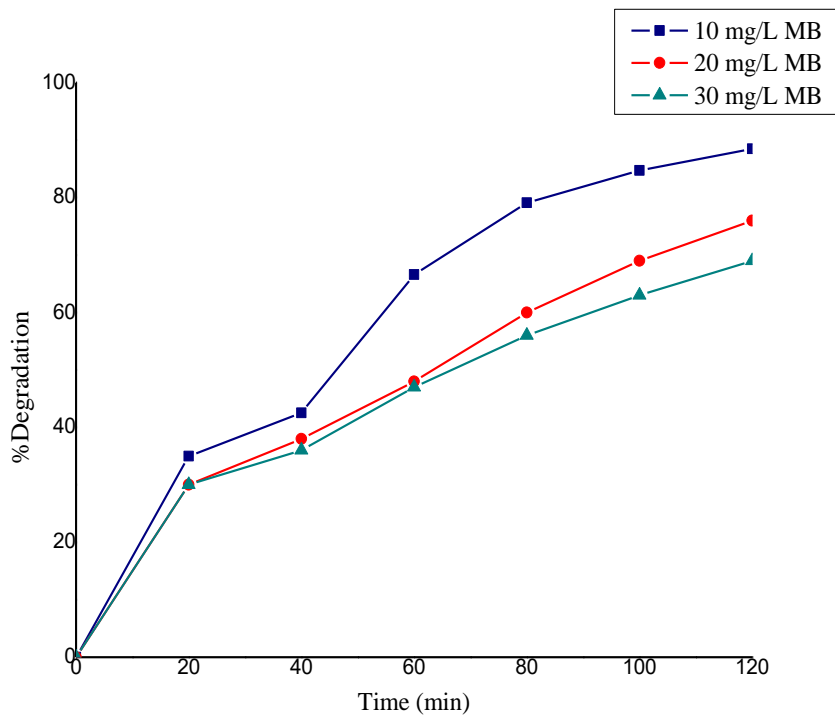


Figure 19: Effect of the initial concentration of MB dye on the degradation efficiency (%) at pH 9 and 30 mg Ag/CuO NCs

4.6. Reusability of the photocatalyst

The reusability of prepared nanocomposites were appraised for the degradation of MB dye in the optimized reaction conditions. The reusability test results for the Ag/CuO NCs catalyst were illustrated in (Fig. 20).

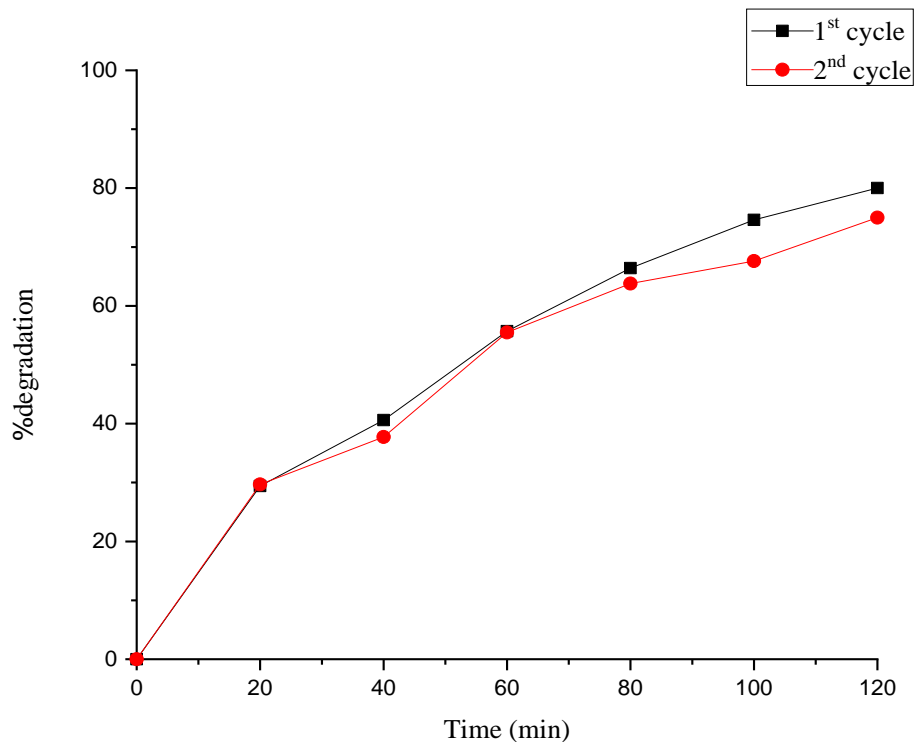


Figure 20: Reusability test of Ag/CuO NCS

The catalytic experiments were carried out under similar conditions, indicating that Ag/CuO NCs have a relatively good activity even in the 2nd cycle. It was shown that the Ag/CuO NCs can maintain their catalytic activity within 80% conversion after two cycles, showed that there was no large reduction of catalytic activity. However, in both cycles there was a slight decrease in the conversion of about 3% and 8.5% respectively. This may be due to the reduction of catalyst dose during the recovery process or either the reactant or the products might undergo adsorption on the surface of the catalyst thereby deactivating the surface activity of the catalyst [12].

4.7. Antibacterial Activity

The result of the antibacterial test was shown in tables 3 and 4.

Table 3: Effect of CuO NPs on selected bacteria (*Salmonella typhaea*, *Bacillus cereus*, *staphylococcus aureus*, and *Escherichia coli* at different concentrations.

Concentration of CuO NPs (mg/ml), PE, and Gentamicin	Zone of inhibition (mm)			
	<i>S. aureus</i>	<i>S. typhi</i>	<i>E. coli</i>	<i>B. cereus</i>
100	23.2±0.28	19.66±1	19.3±0.7	21±0.5
75	18±0.5	15±0.52	16.6±0.5	17±0.14
50	17.8±0.57	13.2±0.28	9±0.5	12±0.86
25	11±0.52	11±0.5	8±0.5	9±0.57
Plant extract	10	7	8	9
DMSO	NI	NI	NI	NI
Gentamicin	19±0.86	20.3±0.57	18±1	20.8±0.57

Table 4: Effect of Ag/CuO NCs on selected bacteria's (*Salmonella typhaea*, *Bacillus cereus*, *staphylococcus aureus* and *E.coli*) at different concentrations

Concentration of Ag/CuO NCs (mg/ml), PE, and Gentamicin	Zone of Inhibition (mm)			
	<i>S. aureus</i>	<i>S. typhi</i>	<i>E. coli</i>	<i>B. cereus</i>
100	25±0.28	20.66±1	20.3±0.76	23±0.5
75	23.16±0.14	15.25±0.25	20±0.28	17.08±0.52
50	20±0.57	13.8±0.5	17±1	17.66±1.15
25	19±0.57	11.5±0.43	10±0.5	10.33±0.71
Plant extract	10	7	7	9
DMSO	NI	NI	NI	NI
Gentamycin	20.6±0.57	20.3±0.57	19.66±1	21.6±0.57

Note: NI= No inhibition, PE= Plant extract

In this study, Ag/CuO NCs showed the highest zone of inhibition against all bacterial strains compared to CuO NPs at all concentrations (Tables 3 and 4, Appendix 10 A). This high antibacterial activity Ag/CuO NCs is due to the high affinity of silver ions for the sulfur in the thiol protein of bacteria. This affinity leads to the breakage of disulfide bonds in thiols that resulted in disruption of protein tertiary structure and causes cell death [141]. This finding was in agreement with [23, 43] that doping of metals (Ag, Zn, Zr, Ce) to CuO NPs increases its antibacterial activity. Additionally, as the concentration of both CuO and Ag/CuO NCs increased from 25 to 100 mg/mL, their antibacterial activity was also increased since the antibacterial activity is concentration-dependent that agreeing with the previous reports [142, 143].

The findings of this study also revealed that gram-positive bacterial strains *Staphylococcus aureus* and *Bacillus cereus* were more sensitive than gram-negative strains *E. coli* and *salmonella typhoea* against the biosynthesized Ag/CuO NCs and CuO NPs and towards plant extract. This variation in the sensitivity or resistance to both gram-positive and gram-negative bacterial populations might be due to the differences in the cell structure, physiology, metabolism, or degree of contact of organisms with nanoparticles [144].

For example, the greater sensitivity of those gram-positive bacteria such as *B. cereus* and *S. aureus* to the CuO NPs and Ag/CuO NCs has been attributed to the greater abundance of amines and carboxyl groups on their cell surface and greater affinity of copper and silver ions towards these groups. Alternatively, gram-negative bacteria like *E.coli* have lipopolysaccharides which possess an important ability to resist antimicrobial agents [145]. These findings were in agreement with recent reports [23, 146] that revealed gram-positive bacteria were more sensitive than gram-negative bacteria.

The synthesized nanoparticles and nanocomposites are highly efficient than Gentamycin except at 50 and 25 mg/mL CuO nanoparticle and Ag/CuO nanocomposites is highly efficient than Gentamicin except at lower concentration (25 mg/mL) since the antimicrobial activity of a CuO NPs depends on concentration and size [23]. Antibacterial activity is also size-dependent; means, if we take both bulk $\text{Cu}(\text{NO}_3)_2 \cdot 3\text{H}_2\text{O}$ and AgNO_3 (Table A) in Appendix 10B), they have antibacterial activity, but their efficiency is less than their corresponding nanoparticles and nanocomposites.

As an example, the Zone of inhibition of Ag/CuO NCs and CuO NPs at higher concentrations (100 mg/mL) for *Staphylococcus aureus* are (25±0.28 and 23.2±0.28 mm) respectively. However, for bulk Ag⁺ and Cu⁺², it was reduced to 16 and 15.25 mm respectively. This indicated that antibacterial activity depends on size, which means as the size decreases surface area of the particle increased, and antibacterial activity increased [12].

Generally, since the size of bulk AgNO₃ and Cu(NO₃)₂.3H₂O is greater than Ag/CuO NCs and CuO NPs, their antibacterial activity is less than their corresponding nanomaterials. The smaller the size of fabricated particles, the higher the oxide content due to the larger surface area. The presence of oxide on the surface ensures the high antibacterial activity of Ag and CuO NPs, most probably due to the higher concentration of ROS, hydrogen peroxide (H₂O₂), superoxide anion (O₂^{•-}), and hydroxyl radical (OH[•]) inside the bacterial cell [147, 148]. Therefore, the enhanced antibacterial activity of Ag/CuO NCs and CuO NPs compared to bulk material is attributed to the large surface area that provides more surface contact with bacteria [149].

The antimicrobial activities of *Ocimum lamiifolium* extract obtained from the aqueous solution against the selected bacterial species were also tested. Zones of inhibitions measured against this aqueous extract were 10, 7, 7, 9 mm for *S. aureus*, *E.coli*, *S .typhae*, and *B. cereus* respectively. The growth zone of inhibition formed by plant extract is lower than both CuO NPs and Ag/CuO NCs because the synthesized nanoparticle enhances the antibacterial activity of plant extract. Furthermore, the zone of inhibition formed by plant extract in this study is lower than the result obtained by literature [19] that reported growth zone of inhibition for *E.coli* 13.5 mm and for *S. aureus* 12 mm. This variation may be due to the difference in the solvent used during extraction since it can vary the biological activity of extract [88]. Additionally, due to the synergetic effect antibacterial activity of synthesized nanoparticles are greater than their corresponding salt and plant extract. Generally, the bactericidal effectiveness of CuO NPs and Ag/CuO NCs has been traced to the development of highly reactive oxygen species such as (OH[•], H₂O₂ and O₂^{•-}) on the surface of the CuO NPs and Ag/CuO NCs, which causes the death to the bacteria [112].

CONCLUSION AND RECOMMENDATIONS

5.1. Conclusion

In this study, CuO NPs and Ag/CuO NCs were successfully synthesized from copper nitrate and silver nitrate using *ocimum lamiifolium* plant extract as a capping and reducing agent. The synthesized nanomaterials were characterized by UV-Vis, FT-IR, SEM, and XRD. The Synthesis of Ag/CuO nanocomposites were optimized by some parameters like pH, metal ion concentration, the volume of extract, temperature, and reaction time to identify the effect of those parameters on the surface synthesis of the nanocomposite. The FT-IR spectroscopy revealed the presence of possible functional groups in the synthesized CuO NPs and Ag/CuO NCs that played as capping and reducing agent. The XRD result showed the synthesized nanomaterials have a crystalline structure. SEM shows CuO NPs has a spherical shape and Ag/CuO NCs has a mixture of spherical and rod-like shape. The effect of parameters like catalyst dose, dye concentration, and pH on the photocatalytic degradation of MB dye was studied and optimized. 30 mg of Ag/CuO NCs and pH 9 was taken as an optimum condition to study the best catalytic performance of the synthesized nanocomposite at 120 min. Ag/CuO NCs (88.5%) showed better degradation efficiency than CuO NPs (76.2%) at optimum conditions due to reduced electron-hole recombination. Photocatalytic degradation of Ag/CuO NCs and CuO NPs was more efficient than photolysis (degradation without catalyst). The synthesized Ag/CuO NCs and CuO NPs have been exhibited significant antibacterial activity against all four bacterial strains. The synthesized nanocomposites and nanoparticles revealed greater antibacterial activity against gram-positive bacteria than gram-negative bacteria. This variation in antibacterial activity is due to differences in their cell structures. The synthesized CuO NPs and Ag/CuO NCs have greater antibacterial activities than *ocimum lamiifolium* leaf extract and their corresponding salt. Generally, *ocimum lamiifolium* leaf extract mediated synthesis of CuO NPs and Ag/CuO nanocomposite have significant application for photocatalytic degradation of MB dye, and as an antibacterial agent against human pathogenic bacteria.

5.2. Recommendation

For further work, the following points were forwarded as recommendations:

- Further characterization is required for the determination of size and composition of the sample using instruments like TEM, SEM, Zeta potential, XPS and EDX.
- Ag/CuO NCs should be applied for the degradation of other types of pollutants.
- The degraded products of MB must be analyzed for identification.
- Further research work is required on some other metal-doped, metal oxide nanoparticles through the mediation of *Ocimum lamiifolium* leaf extract with an application of their antibacterial agents and photocatalytic activity.
- Finally, the antibacterial effects of Ag/CuO NCs against some other bacteria must be studied.

6. REFERENCES

- [1] Belver, C.; Bellod, R.; Fuerte, A.; Fernández-García, M. Nitrogen-Containing TiO₂ Photocatalysts. Part 1. Synthesis and Solid Characterization. *Appl. Catal. B Environ.* **2006**, *65*, 301–308.
- [2] Wang, X.; Gu, X.; Lin, D.; Dong, F.; Wan, X. Treatment of Acid Rose Dye Containing Wastewater by Ozonizing - Biological Aerated Filter. *Dye. Pigment.* **2007**, *74*, 736–740.
- [3] Husain, Q. Potential Applications of the Oxidoreductive Enzymes in the Decolorization and Detoxification of Textile and Other Synthetic Dyes from Polluted Water: A Review. *Crit. Rev. Biotechnol.* **2006**, *26*, 201–221.
- [4] Al-Hakkani, M. F. Biogenic Copper Nanoparticles and Their Applications: A Review. *SN Appl. Sci.* **2020**.
- [5] Llor, C.; Bjerrum, L. Antimicrobial Resistance: Risk Associated with Antibiotic Overuse and Initiatives to Reduce the Problem. *Ther. Adv. Drug Saf.* **2014**, *5*, 229–241.
- [6] Fair, R. J.; Tor, Y. Antibiotics and Bacterial Resistance in the 21st Century. *Perspect. Medicin. Chem.* **2014**, *6*, 25–64.
- [7] Kazemian, H.; Ghafourian, S.; Heidari, H.; Amiri, P.; Yamchi, J. K.; Shavalipour, A.; Houri, H.; Maleki, A.; Sadeghifard, N. Antibacterial, Anti-Swarming and Anti-Biofilm Formation Activities of *Chamaemelum Nobile* against *Pseudomonas Aeruginosa*. *Rev. Soc. Bras. Med. Trop.* **2015**, *48*, 432–436.
- [8] Taylor, E.; Webster, T. J. Reducing Infections through Nanotechnology and Nanoparticles. **2011**, 1463–1473.
- [9] Akintelu, S. A.; Folorunso, A. S.; Folorunso, F. A.; Oyebamiji, A. K. Green Synthesis of Copper Oxide Nanoparticles for Biomedical Application and Environmental Remediation. *Heliyon.* **2020**, *6*, 4508.
- [10] Pakzad, K.; Alinezhad, H.; Nasrollahzadeh, M. Green Synthesis of Ni @ Fe₃O₄ and CuO Nanoparticles Using *Euphorbia Maculata* Extract as Photocatalysts for the Degradation of Organic Pollutants under UV-Irradiation. *Ceram. Int.* **2019**, *45*, 17173–17182.
- [11] Singh, J.; Rawat, M. A Brief Review on Synthesis and Characterization of Copper Oxide Nanoparticles and Its Applications. **2016**.
- [12] Buazar, F.; Sweidi, S.; Badri, M.; Kroushawi, F. Biofabrication of Highly Pure Copper Oxide Nanoparticles Using Wheat Seed Extract and Their Catalytic Activity: A Mechanistic Approach. *Green Process. Synth.* **2019**, *8*, 691–702.
- [13] Online, V. A.; Saboury, A. A.; Davar, F.; Semnani, A. RSC Advances. **2016**.
- [14] Singh, J.; Dutta, T.; Kim, K. H.; Rawat, M.; Samddar, P.; Kumar, P. “Green” Synthesis of Metals and Their Oxide Nanoparticles: Applications for Environmental Remediation. *J. Nanobiotechnology.* **2018**, *16*, 1–24.
- [15] Nasrollahzadeh, M.; Ghorbannezhad, F.; Issaabadi, Z.; Sajadi, S. M. Recent Developments in the Biosynthesis of Cu-Based Recyclable Nanocatalysts Using Plant

- Extracts and Their Application in the Chemical Reactions. **2019**, 3, 601–643.
- [16] Similoluwa, F. A. Characterization and Antimicrobial Investigation of Synthesized Silver Nanoparticles Characterization and Antimicrobial Investigation of Synthesized Silver Nanoparticles from *Annona Muricata* Leaf Extracts. **2019**.
- [17] Raizada, P.; Sudhaik, A.; Patial, S.; Hasija, V.; Parwaz Khan, A. A.; Singh, P.; Gautam, S.; Kaur, M.; Nguyen, V. H. Engineering Nanostructures of CuO-based Photocatalysts for Water Treatment: Current Progress and Future Challenges. *Arab. J. Chem.* **2020**, 13, 8424–8457.
- [18] Arya, S.; Singh, A.; Kour, R. Comparative Study of CuO , CuO @ Ag and CuO @ Ag : La Nanoparticles for Their Photosensing Properties Comparative Study of CuO, CuO @ Ag and CuO @ Ag : La nanoparticles for their Photosensing Properties. **2019**.
- [19] Ambaye, T. G. In Vitro Antimicrobial Efficacy of Fractions from Demakese (*Ocimum Lamifolium*) Leaves Extract from Mekelle Tigra. **2018**.
- [20] Sahalie, N. A.; Abrha, L. H.; Tolesa, L. D.; Rakitin, O. Lamiifolium (Damakese) as a Treatment for Urinary Tract Infection Chemical Composition and Antimicrobial Activity of Leave Extract of *Ocimum Lamiifolium* (Damakese) as a Treatment for Urinary Tract Infection. *Cogent Chem.* **2018**, 4, 1–10.
- [21] Rajendaran, K.; Muthuramalingam, R.; Ayyadurai, S. Green Synthesis of Ag-Mo/CuO Nanoparticles Using *Azadirachta Indica* Leaf Extracts to Study Its Solar Photocatalytic and Antimicrobial Activities. *Mater. Sci. Semicond. Process.* **2019**, 9, 230–238.
- [22] Jadhav, M. S.; Kulkarni, S.; Raikar, P.; Barretto, D. A. And Evaluation of Antibacterial , Antioxidant And. **2018**, 204–213.
- [23] Kumar, K. K. P.; Dinesh, N. D.; Murari, S. K. Synthesis of CuO and Ag Doped CuO Nanoparticles from *Muntingia Calabura* Leaf Extract and Evaluation of Their Antimicrobial Potential. *Int. J. Nano Biomater.* **2019**, 8, 228–252.
- [24] Motahari, F.; Mozdianfard, M. R.; Soofivand, F.; Salavati-Niasari, M. NiO Nanostructures: Synthesis, Characterization and Photocatalyst Application in Dye Wastewater Treatment. *RSC Adv.* **2014**, 4, 27654–27660.
- [25] Khairnar, S. D.; Shrivastava, V. S. Facile Synthesis of Nickel Oxide Nanoparticles for the Degradation of Methylene Blue and Rhodamine B Dye: A Comparative Study. *J. Taibah Univ. Sci.* **2019**, 13, 1108–1118.
- [26] Nandhini, N. T.; Rajeshkumar, S.; Mythili, S. The Possible Mechanism of Eco-Friendly Synthesized Nanoparticles on Hazardous Dyes Degradation. *Biocatal. Agric. Biotechnol.* **2019**, 19, 101-138.
- [27] Chauhan, M.; Kaur, N.; Bansal, P.; Kumar, R.; Srinivasan, S.; Chaudhary, G. R. Proficient Photocatalytic and Sonocatalytic Degradation of Organic Pollutants Using CuO Nanoparticles. *J. Nanomater.* **2020**.
- [28] Phang, Y. K.; Aminuzzaman, M.; Akhtaruzzaman, M.; Muhammad, G.; Ogawa, S.; Watanabe, A.; Tey, L. H. Green Synthesis and Characterization of CuO Nanoparticles

- Derived from Papaya Peel Extract for the Photocatalytic Degradation of Palm Oil Mill Effluent (POME). *Sustain.* **2021**, *13*, 1–15.
- [29] Aragaw, T. A.; Bogale, F. M.; Aragaw, B. A. Iron-Based Nanoparticles in Wastewater Treatment: A Review on Synthesis Methods, Applications, and Removal Mechanisms. *J. Saudi Chem. Soc.* **2021**, *25*, 101280.
- [30] Mba, I. E.; Nweze, E. I. Nanoparticles as Therapeutic Options for Treating Multidrug-Resistant Bacteria: Research Progress, Challenges, and Prospects. *World J. Microbiol. Biotechnol.* **2021**, *37*, 1–30.
- [31] AlMatar, M.; Makky, E. A.; Var, I.; Koksai, F. The Role of Nanoparticles in the Inhibition of Multidrug-Resistant Bacteria and Biofilms. *Curr. Drug Deliv.* **2017**.
- [32] Baig, N.; Kammakakam, I.; Falath, W.; Kammakakam, I. Nanomaterials: A Review of Synthesis Methods, Properties, Recent Progress, and Challenges. *Mater. Adv.* **2021**, *2*, 1821–1871.
- [33] Jeevanandam, J.; Barhoum, A.; Chan, Y. S.; Dufresne, A.; Danquah, M. K. Review on Nanoparticles and Nanostructured Materials: History, Sources, Toxicity and Regulations. **2018**, 1050–1074.
- [34] Pourfath, M. Encyclopedia of Nanoscience and Nanotechnology. *Choice Rev. Online.* **2005**, *42*, 42-2552.
- [35] Senapati, S. Biosynthesis and Immobilization of Nanoparticles and Their Applications. *Ph. D, thesis.* **2005**, 1–171.
- [36] Patra, J. K.; Baek, K. Green Nanobiotechnology: Factors Affecting Synthesis and Characterization Techniques. **2014**.
- [37] Harishchandra, B. D.; Pappuswamy, M.; Pu, A.; Shama, G.; Pragatheesh, A.; Arumugam, V. A.; Sundaram, R. Copper Nanoparticles: A Review on Synthesis, Characterization and Applications. **2020**, *5*, 201–210.
- [38] Zhou, Y.; Lin, W.; Huang, J. Biosynthesis of Gold Nanoparticles by Foliar Broths: Roles of Biocompounds and Other Attributes of the Extracts. **2010**, 1351–1359.
- [39] Makarov, V. V.; Love, A. J.; Sinitsyna, O. V.; Makarova, S. S.; Yaminsky, I. V. “Green” Nanotechnologies: Synthesis of Metal Nanoparticles Using Plants. **2014**, *6*, 35–44.
- [40] Lade, B. D.; Shanware, A. S. Phytonanofabrication: Methodology and Factors Affecting Biosynthesis of Nanoparticles. **2020**, 1-7.
- [41] Nagajyothi, P. C.; Vattikuti, S. V. P.; Devarayapalli, K. C.; Yoo, K.; Sreekanth, T. V. M.; Vattikuti, S. V. P.; Devarayapalli, K. C.; Yoo, K. Green Synthesis: Photocatalytic Degradation of Textile Dyes Using Metal and Metal Oxide Nanoparticles-Latest. *Crit. Rev. Environ. Sci. Technol.* **2019**, *10*, 1–107.
- [42] Palem, R. R.; Ganesh, S. D.; Kronekova, Z.; Sláviková, M.; Saha, N.; Saha, P. Green Synthesis of Silver Nanoparticles and Biopolymer Nanocomposites: A Comparative Study on Physico-Chemical, Antimicrobial and Anticancer Activity. *Bull. Mater. Sci.*

2018.

- [43] Parvathiraja, C.; Shailajha, S. Bioproduction of CuO and Ag/CuO Heterogeneous Photocatalysis-Photocatalytic Dye Degradation and Biological Activities. *Appl. Nanosci.* **2021**, *11*, 1411–1425.
- [44] Elemike, E. E.; Onwudiwe, D. C.; Ogeleka, D. F.; Mbonu, J. I. Phyto-Assisted Preparation of Ag and Ag–CuO Nanoparticles Using Aqueous Extracts of *Mimosa Pigra* and Their Catalytic Activities in the Degradation of Some Common Pollutants. *J. Inorg. Organomet. Polym. Mater.* **2019**, *29*, 1798–1806.
- [45] Manuscript, A. Rsc.Li/Njc. **2017**.
- [46] Links, D. A. Green Chemistry Green Synthesis of Metal Nanoparticles Using Plants. **2011**, 2638–2650.
- [47] Abu-dief, A. M. Development of Metal Oxide Nanoparticles as Semiconductors. **2020**, *1* (1), 5–10.
- [48] Anandan, S.; Lee, G.; Wu, J. J. Ultrasonics Sonochemistry Sonochemical Synthesis of CuO Nanostructures with Different Morphology. *Ultrason-Sonochemistry.* **2012**, *19*, 682–686.
- [49] Mobasser, S.; Akbar Firoozi, A. Review of Nanotechnology Applications in Science and Engineering. *J. homepage www.ojceu.ir J. Civ. Eng. Urban.* **2016**, *6*, 84–93.
- [50] Dontsova, T. A.; Nahirniak, S. V.; Astrelin, I. M. Metaloxide Nanomaterials and Nanocomposites of Ecological Purpose. *J. Nanomater.* **2019**.
- [51] Yaqoob, A. A.; Ahmad, H.; Parveen, T.; Ahmad, A.; Oves, M. Recent Advances in Metal Decorated Nanomaterials and Their Various Biological Applications : A Review. **2020**, *8*, 1–23.
- [52] Mallakpour, S.; Azadi, E.; Hussain, C. M. The Latest Strategies in the Fight against the COVID-19 Pandemic: The Role of Metal and Metal Oxide Nanoparticles. *New J. Chem.* **2021**, *45*, 6167–6179.
- [53] Asere, T. G.; Laing, G. Du. Zn-Doped CdSe Nanoparticles: Impact of Synthesis Conditions on Photocatalytic Activity. *Environ. Technol. Innov.* **2020**, *20*, 101-126.
- [54] William, W.; Oppong, S. O. B.; Oppong, O. B.; Anku, W.; Govender, P. P.; Govender, P. Bismuth-Based Nanoparticles as Photocatalytic Materials Materials. **2018**.
- [55] Singh, R.; Smitha, M. S.; Singh, S. P. The Role of Nanotechnology in Combating Multi-Drug Resistant Bacteria. **2014**, *14*, 4745–4756.
- [56] Cavassin, E. D.; Francisco, L.; Figueiredo, P. De; Otoch, J. P.; Seckler, M. M.; Oliveira, R. A. De; Franco, F. F.; Marangoni, V. S.; Zucolotto, V.; Sara, A.; et al. Comparison of Methods to Detect the in Vitro Activity of Silver Nanoparticles against Multidrug Resistant Bacteria. *J. Nanobiotechnology.* **2015**, 1–16.
- [57] Wang, S.; Lawson, R.; Ray, P. C.; Yu, H. Toxic Effects of Gold Nanoparticles on Salmonella Typhimurium Bacteria. **2011**.

- [58] Beyth, N.; Hour-Haddad, Y.; Domb, A.; Khan, W.; Hazan, R. Alternative Antimicrobial Approach: Nano-Antimicrobial Materials. *Evidence-based Complement. Altern. Med.* **2015**.
- [59] Yedurkar, S. M.; Maurya, C. B.; Mahanwar, P. A. A Biological Approach for the Synthesis of Copper Oxide Nanoparticles by *Ixora Coccinea* Leaf Extract. **2017**, *8*, 1173–1178.
- [60] Delgado, A.; Corni, S.; Goldoni, G.; Delgado, A.; Corni, S.; Goldoni, G. Modeling Opto-Electronic Properties of a Dye Molecule in Proximity of a Semiconductor Nanoparticle. **2013**.
- [61] Ansilin, S.; Nair, J. K.; Aswathy, C.; Rama, V.; Peter, J.; Persis, J. J.; Tucker, S.; Autonomous, C. Green Synthesis and Characterisation of Copper Oxide Nanoparticles Using *Azadirachta Indica* (Neem) Leaf Aqueous Extract. *J. Nanosci. Technol.* **2016**, *2*, 221–223.
- [62] Baudot, C.; Ming, C.; Chien, J. Infrared Physics & Technology FTIR Spectroscopy as a Tool for Nano-Material Characterization. *Infrared Phys. Technol.* **2010**, *53*, 434–438.
- [63] Press, D. One-Step Green Synthesis and Characterization of Leaf Extract-Mediated Biocompatible Silver and Gold Nanoparticles from *Memecylon Umbellatum*. **2013**, 1307–1315.
- [64] Birkholz, M. *Thin Film Analysis by X-Ray Scattering*. **2006**.
- [65] Bunaciu, A. A.; Udriștioiu, E.; Aboul-enein, H. Y.; Bunaciu, A. A.; Udriștioiu, E.; Aboul-enein, H. Y.; Bunaciu, A. A.; S, E. G. U. Critical Reviews in Analytical Chemistry X-Ray Diffraction: Instrumentation and Applications X-Ray Diffraction: Instrumentation and Applications. **2015**, 8347.
- [66] Jensen, H.; Pedersen, J. H.; J, J. E.; Pedersen, J. S.; Joensen, K. D.; Iversen, S. B.; S, E. G.; Pedersen, J. H.; J, J. E.; Pedersen, J. S. Determination of Size Distributions in Nanosized Powders by TEM, XRD, and SAXS. **2007**.
- [67] Sharma, S. K.; Verma, D. S.; Khan, L. U.; Kumar, S.; Khan, S. B. *Handbook of Materials Characterization*. **2018**.
- [68] Liu, J. Scanning Transmission Electron Microscopy and Its Application to the Study of Nanoparticles and Nanoparticle Systems. *J. Electron Microsc. (Tokyo)*. **2005**, *54*, 251–278.
- [69] Nordin, N. R.; Shamsuddin, M. Biosynthesis of Copper (II) Oxide Nanoparticles Using *Murayya Koeniggi* Aqueous Leaf Extract and Its Catalytic Activity in 4-Nitrophenol Reduction. **2019**, *15*, 2–8.
- [70] Renuga, D.; Jeyasundari, J.; Athithan, A. S. S.; Jacob, Y. B. A. Synthesis and Characterization of Copper Oxide Nanoparticles Using *Brassica Oleracea Var* Extract for Its Antifungal Application. **2020**.
- [71] Ismail, A. M.; Mohamed, E. A.; Marghany, M. R.; Abdel-Motaal, F. F.; Abdel-Farid, I. B.; El-Sayed, M. A. Preliminary Phytochemical Screening, Plant Growth Inhibition and

- Antimicrobial Activity Studies of Faidherbia Albida Legume Extracts. *J. Saudi Soc. Agric. Sci.* **2016**, *15*, 112–117.
- [72] Sadeghi, B.; Rostami, A.; Momeni, S. S. Spectrochimica Acta Part A : Facile Green Synthesis of Silver Nanoparticles Using Seed Aqueous Extract of Pistacia Atlantica and Its Antibacterial Activity. **2015**, *134*, 326–332.
- [73] Lartey, P. A.; Nellans, H. N.; Tanaka, S. K. *New Developments in Macrolides: Structures and Antibacterial and Prokinetic Activities.* **1994**.
- [74] Vaidehi, D.; Bhuvaneshwari, V.; Khashan, K. S.; Jabir, M. S. Biosynthesis of Copper Oxide Nanoparticles from *Drypetes Sepiaria* Leaf Extract and Their Catalytic Activity to Dye Degradation. **2017**.
- [75] Kayani, Z. N.; Aslam, H. Examination of the Properties of Doped Copper Oxide by Silver : Prepared Chemical Method. **2019**.
- [76] Iqbal, S.; Javed, M.; Bahadur, A.; Qamar, M. A.; Ahmad, M.; Shoaib, M.; Raheel, M.; Ahmad, N.; Akbar, M. B.; Li, H. Controlled Synthesis of Ag-Doped CuO Nanoparticles as a Core with Poly(Acrylic Acid) Microgel Shell for Efficient Removal of Methylene Blue under Visible Light. *J. Mater. Sci. Mater. Electron.* **2020**, *31*, 8423–8435.
- [77] Thamer, N. A.; Muftin, N. Q.; Al-Rubae, S. H. N. Optimization Properties and Characterization of Green Synthesis of Copper Oxide Nanoparticles Using Aqueous Extract of Cordia Myxa L. Leaves. *Asian J. Chem.* **2018**, *30*, 1559–1563.
- [78] Ijaz, F.; Shahid, S.; Khan, S. A.; Ahmad, W. Green Synthesis of Copper Oxide Nanoparticles Using *Abutilon Indicum* Leaf Extract : Antimicrobial , Antioxidant and Photocatalytic Dye Degradation Activities. **2017**, *16*, 743–753.
- [79] Hemalatha, S.; Makeswari, M. Photocatalytic Degradation of Vat Red 13 by Green Synthesized Copper Oxide Nanocatalyst. **2018**, *16*, 1–8.
- [80] Yibeltal, A. W.; Beyene, B. B.; Admassie, S.; Tadesse, A. M.; Dar, B.; Program, M. S.; Box, P. O.; Ababa, A.; Dawa, D. **2020**, *34*, 55–66.
- [81] Kosmulski, M. The PH Dependent Surface Charging and Points of Zero Charge. VI. Update. *J. Colloid Interface Sci.* **2014**, *426*, 209–212.
- [82] Bakatula, E. N.; Richard, D.; Neculita, C. M.; Zagury, G. J. Determination of Point of Zero Charge of Natural Organic Materials. *Environ. Sci. Pollut. Res.* **2018**, *25*, 7823–7833.
- [83] Shamsuddin, M.; Raja Nordin, N. Biosynthesis of Copper(II) Oxide Nanoparticles Using *Murayya Koeniggi* Aqueous Leaf Extract and Its Catalytic Activity in 4-Nitrophenol Reduction. *Malaysian J. Fundam. Appl. Sci.* **2019**, *15*, 218–224.
- [84] Taghavi Fardood, S.; Forootan, R.; Moradnia, F.; Afshari, Z.; Ramazani, A. Green Synthesis, Characterization, and Photocatalytic Activity of Cobalt Chromite Spinel Nanoparticles. *Mater. Res. Express.* **2020**.
- [85] Divya, K.; Ramalakshmi, K.; Murthy, P. S.; Jagan Mohan Rao, L. Volatile Oils from

- Ferula Asafoetida Varieties and Their Antimicrobial Activity. *LWT - Food Sci. Technol.* **2014**, *59*, 774–779.
- [86] Hiruy, M.; Bisrat, D.; Mazumder, A.; Asres, K. Two Chromones with Antimicrobial Activity from the Leaf Latex of Aloe Monticola Reynolds. *Nat. Prod. Res.* **2021**, *35*, 1052–1056.
- [87] Balouiri, M.; Sadiki, M.; Ibsouda, S. K. Methods for in Vitro Evaluating Antimicrobial Activity: A Review. *J. Pharm. Anal.* **2016**, *6*, 71–79.
- [88] Cieniak, C.; Walshe-Roussel, B.; Liu, R.; Muhammad, A.; Saleem, A.; Haddad, P. S.; Cuerrier, A.; Foster, B. C.; Arnason, J. T. Phytochemical Comparison of the Water and Ethanol Leaf Extracts of the Cree Medicinal Plant, Sarracenia Purpurea L. (Sarraceniaceae). *J. Pharm. Pharm. Sci.* **2015**, *18*, 484–493.
- [89] De Toledo, L. de A. S.; Rosseto, H. C.; Bruschi, M. L. Iron Oxide Magnetic Nanoparticles as Antimicrobials for Therapeutics. *Pharm. Dev. Technol.* **2018**, *23*, 316–323.
- [90] Christopher, J. S. G.; Saswati, B.; Ezilrani, P. S. Optimization of Parameters for Biosynthesis of Silver Nanoparticles Using Leaf Extract of *Aegle Marmelos*. *Brazilian Arch. Biol. Technol.* **2015**, *58*, 702–710.
- [91] Eya'ane Meva, F.; Segnou, M. L.; Ebongue, C. O.; Ntomba, A. A.; Kedi, P. B. E.; Deli, V.; Etoh, M. A.; Mpondo, E. M. Spectroscopic Synthetic Optimizations Monitoring of Silver Nanoparticles Formation from Megaphrynum Macrostachyum Leaf Extract. *Rev. Bras. Farmacogn.* **2016**, *26*, 640–646.
- [92] Letchumanan, D.; Sok, S. P. M.; Ibrahim, S.; Nagoor, N. H.; Arshad, N. M. Plant-Based Biosynthesis of Copper/Copper Oxide Nanoparticles: An Update on Their Applications in Biomedicine, Mechanisms, and Toxicity. *Biomolecules.* **2021**.
- [93] Salvadori, M. R.; Ando, R. A.; Nascimento, C. A. O.; Corrêa, B. Extra and Intracellular Synthesis of Nickel Oxide Nanoparticles Mediated by Dead Fungal Biomass. *PLoS One.* **2015**, *10*, 1–15.
- [94] Gnanaprakasam, A.; Sivakumar, V. M.; Thirumarimurugan, M. A Study on Cu and Ag Doped ZnO Nanoparticles for the Photocatalytic Degradation of Brilliant Green Dye: Synthesis and Characterization. *Water Sci. Technol.* **2016**, *74*, 1426–1435.
- [95] Tan, T. L.; Lai, C. W.; Abd Hamid, S. B. Tunable Band Gap Energy of Mn-Doped ZnO Nanoparticles Using the Coprecipitation Technique. *J. Nanomater.* **2014**.
- [96] Hulkoti, N. I.; Taranath, T. C. Biosynthesis of Nanoparticles Using Microbes-A Review. *Colloids Surfaces B Biointerfaces.* **2014**, *121*, 474–483.
- [97] Chen, M. N.; Chan, C. F.; Huang, S. L.; Lin, Y. S. Green Biosynthesis of Gold Nanoparticles Using *Chenopodium Formosanum* Shell Extract and Analysis of the Particles' Antibacterial Properties. *J. Sci. Food Agric.* **2019**, *99*, 3693–3702.
- [98] Upadhyay, L. S. B.; Kumar, N. Green Synthesis of Copper Nanoparticle Using Glucose and Polyvinylpyrrolidone (PVP). *Inorg. Nano-Metal Chem.* **2017**, *47*, 1436–1440.

- [99] Yu, H.; Peng, Y.; Yang, Y.; Li, Z. Y. Plasmon-Enhanced Light–Matter Interactions and Applications. *npj Comput. Mater.* **2019**, *5*, 1–14.
- [100] Benhammada, A.; Trache, D.; Chelouche, S.; Mezroua, A. Catalytic Effect of Green CuO Nanoparticles on the Thermal Decomposition Kinetics of Ammonium Perchlorate. *Zeitschrift für Anorg. und Allg. Chemie.* **2021**, *647*, 312–325.
- [101] Z.I.Takai. *Journal of Asian J. Chem.* **2018**, *30*, 2424–2430.
- [102] Bala, N.; Saha, S.; Chakraborty, M.; Maiti, M.; Das, S.; Basu, R.; Nandy, P. Green Synthesis of Zinc Oxide Nanoparticles Using *Hibiscus Subdariffa* Leaf Extract: Effect of Temperature on Synthesis, Anti-Bacterial Activity and Anti-Diabetic Activity. *RSC Adv.* **2015**, *5*, 4993–5003.
- [103] Patra, J. K.; Baek, K. H. Green Nanobiotechnology: Factors Affecting Synthesis and Characterization Techniques. *J. Nanomater.* **2014**.
- [104] Bukhari, S. I.; Hamed, M. M.; Al-Agamy, M. H.; Gazwi, H. S. S.; Radwan, H. H.; Youssif, A. M. Biosynthesis of Copper Oxide Nanoparticles Using *Streptomyces* MHM38 and Its Biological Applications. *J. Nanomater.* **2021**.
- [105] Ramli, N. A.; Jai, J.; Yusof, N. M. Green Synthesis of Silver Nanoparticles Using *Elaeis Guineensis* (Palm Leaves): An Investigation on the Effect of Reaction Time in Reduction Mechanism and Particle Size. *Appl. Mech. Mater.* **2014**, *575*, 36–40.
- [106] Girma, T.; Du, G. Environmental Technology & Innovation Zn-Doped CdSe Nanoparticles: Impact of Synthesis Conditions on Photocatalytic Activity. *Environ. Technol. Innov.* **2020**, *20*, 101-126.
- [107] Hossain, S. M.; Park, H.; Kang, H. J.; Mun, J. S.; Tijing, L.; Rhee, I.; Kim, J. H.; Jun, Y. S.; Shon, H. K. Facile Synthesis and Characterization of Anatase TiO₂/g-CN Composites for Enhanced Photoactivity under UV–Visible Spectrum. *Chemosphere.* **2021**, *262*, 1280.
- [108] Khojier, K.; Savaloni, H.; Sadeghi, Z. A Comparative Investigation on Growth, Nanostructure and Electrical Properties of Copper Oxide Thin Films as a Function of Annealing Conditions. *J. Theor. Appl. Phys.* **2014**.
- [109] Menazea, A. A.; Mostafa, A. M. Ag Doped CuO Thin Film Prepared via Pulsed Laser Deposition for 4-Nitrophenol Degradation. *J. Environ. Chem. Eng.* **2020**, *8*, 104.
- [110] Ahmad, M. A.; Aslam, S.; Mustafa, F.; Arshad, U. Synergistic Antibacterial Activity of Surfactant Free Ag–GO Nanocomposites. *Sci. Rep.* **2021**, *11*, 1–9.
- [111] Jamkhande, P. G.; Ghule, N. W.; Bamer, A. H.; Kalaskar, M. G. Metal Nanoparticles Synthesis: An Overview on Methods of Preparation, Advantages and Disadvantages, and Applications. *J. Drug Deliv. Sci. Technol.* **2019**, *53*, 101174.
- [112] Babu, A. T.; Antony, R. Green Synthesis of Silver Doped Nano Metal Oxides of Zinc & Copper for Antibacterial Properties, Adsorption, Catalytic Hydrogenation & Photodegradation of Aromatics. *J. Environ. Chem. Eng.* **2019**.
- [113] Batool, M. Studie on Malachite Green Dye Degradation by Biogenic Metal Nano CuO

And CuO/ZnO Nano Composites. *Arch. Nanomedicine Open Access J.* **2018**.

- [114] Zia, F.; Ghafoor, N.; Iqbal, M.; Mehboob, S. Green Synthesis and Characterization of Silver Nanoparticles Using *Cydonia Oblong* Seed Extract. *Appl. Nanosci.* **2016**, *6*, 1023–1029.
- [115] Zeid, E. F. A.; Ibrahim, I. A.; Mohamed, W. A. A.; Ali, A. M. Study the Influence of Silver and Cobalt on the Photocatalytic Activity of Copper Oxide Nanoparticles for the Degradation of Methyl Orange and Real Wastewater Dyes. *Mater. Res. Express.* **2020**.
- [116] Liu, Y. Y.; Liu, X. Y.; Yang, J. M.; Lin, D. L.; Chen, X.; Zha, L. S. Investigation of Ag Nanoparticles Loading Temperature Responsive Hybrid Microgels and Their Temperature Controlled Catalytic Activity. *Colloids Surfaces A Physicochem. Eng. Asp.* **2012**, *393*, 105–110.
- [117] Kokate, M.; Garadkar, K.; Gole, A. Zinc-Oxide-Silica-Silver Nanocomposite: Unique One-Pot Synthesis and Enhanced Catalytic and Anti-Bacterial Performance. *J. Colloid Interface Sci.* **2016**, *483*, 249–260.
- [118] Asamoah, R. B.; Annan, E.; Mensah, B.; Nbelayim, P.; Apalangya, V.; Onwona-Agyeman, B.; Yaya, A. A Comparative Study of Antibacterial Activity of CuO/Ag and ZnO/Ag Nanocomposites. *Adv. Mater. Sci. Eng.* **2020**.
- [119] Nassar, A. M.; Abo Zeid, E. F.; Elseman, A. M.; Alotaibi, N. F. A Novel Heterometallic Compound for Design and Study of Electrical Properties of Silver Nanoparticles-Decorated Lead Compounds. *New J. Chem.* **2018**, *42*, 1387–1395.
- [120] Chandrasekar, A.; Vasantharaj, S.; Jagadeesan, N. L.; Shankar, S. N.; Pannerselvam, B.; Bose, V. G.; Arumugam, G.; Shanmugavel, M. Studies on Phytomolecules Mediated Synthesis of Copper Oxide Nanoparticles for Biomedical and Environmental Applications. *Biocatal. Agric. Biotechnol.* **2021**, *33*, 101994.
- [121] Abdeslam, S. Influence of Silver Inclusions on the Mechanical Behavior of Cu-Ag Nanocomposite during Nanoindentation: Molecular Dynamics Study. *Results Phys.* **2019**, *15*, 102672.
- [122] Ong, C. B.; Ng, L. Y.; Mohammad, A. W. A Review of ZnO Nanoparticles as Solar Photocatalysts: Synthesis, Mechanisms and Applications. *Renew. Sustain. Energy Rev.* **2018**, *81*, 536–551.
- [123] Ghulam, M.; Hajira, T.; Muhammad, S.; Nasir, A. Synthesis and Characterization of Cupric Oxide (CuO) Nanoparticles and Their Application for the Removal of Dyes. *African J. Biotechnol.* **2013**, *12*, 6650–6660.
- [124] Herrmann, J. M. Heterogeneous Photocatalysis: An Emerging Discipline Involving Multiphase Systems. *Catal. Today.* **1995**, *24*, 157–164.
- [125] Darvishi Cheshmeh Soltani, R.; Khataee, A. R.; Mashayekhi, M. Photocatalytic Degradation of a Textile Dye in Aqueous Phase over ZnO Nanoparticles Embedded in Biosilica Nanobiostructure. *Desalin. Water Treat.* **2016**, *57*, 13494–13504.
- [126] Alkaykh, S.; Mbarek, A.; Ali-Shattle, E. E. Photocatalytic Degradation of Methylene Blue

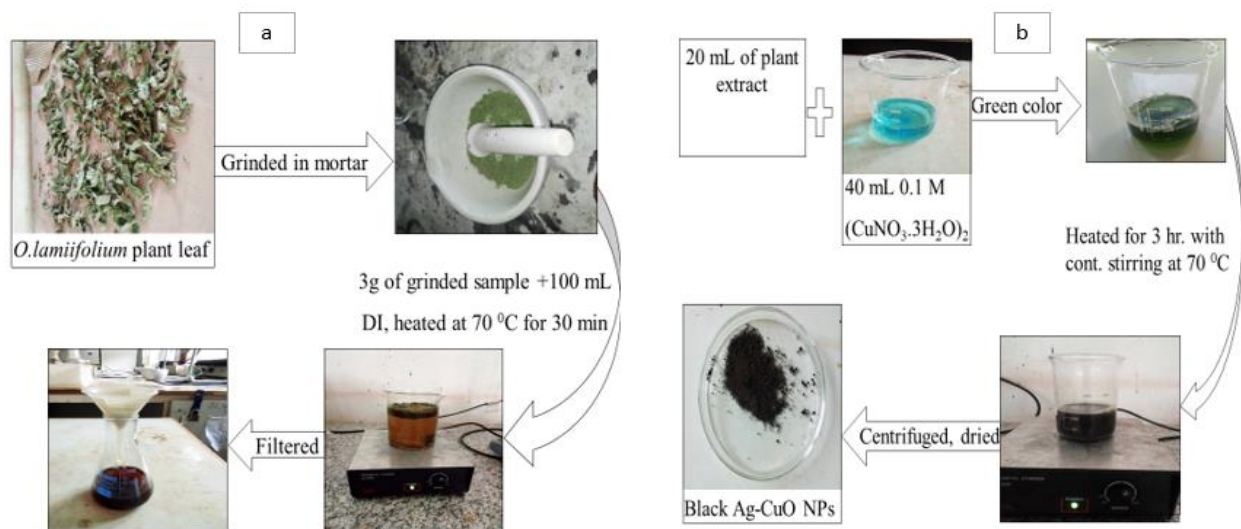
- Dye in Aqueous Solution by MnTiO₃ Nanoparticles under Sunlight Irradiation. *Heliyon*. **2020**, *6*, 3663.
- [127] Janeiro, D. Photocatalytic degradation of Methylene Blue dye from aqueous system by HKUST-1 and CuO@HKUST-1. **2018**, *21*, 1–9.
- [128] Ezgi, E.; Mehmet, A.; Ramazan, A.; Kazim, K.; Lokman, U.; Semran, S.; Feza, K.; Necdet, S. *Plant Nanobionics*. **2019**.
- [129] Ajmal, A.; Majeed, I.; Malik, R. N.; Idriss, H.; Nadeem, M. A. Principles and Mechanisms of Photocatalytic Dye Degradation on TiO₂ Based Photocatalysts: A Comparative Overview. *RSC Adv*. **2014**, *4*, 37003–37026.
- [130] Tang, W. Z.; Huren An. Photocatalytic Degradation Kinetics and Mechanism of Acid Blue 40 by TiO₂/UV in Aqueous Solution. *Chemosphere*. **1995**, *31*, 4171–4183.
- [131] Sajjadi, A.; Hosseini Ravandi, S. A.; Izadan, H.; Kadivar, N. Purification of Methylene Blue via Photocatalytic Nanofibrous Membranes Containing TiO₂ Nanoparticles. *J. Eng. Fiber. Fabr*. **2016**, *11*, 43–55.
- [132] Behnajady, M. A.; Modirshahla, N.; Hamzavi, R. Kinetic Study on Photocatalytic Degradation of C.I. Acid Yellow 23 by ZnO Photocatalyst. *J. Hazard. Mater*. **2006**, *133*, 226–232.
- [133] Nguyen Thi Thu, T.; Nguyen Thi, N.; Tran Quang, V.; Nguyen Hong, K.; Nguyen Minh, T.; Le Thi Hoai, N. Synthesis, Characterisation, and Effect of PH on Degradation of Dyes of Copper-Doped TiO₂. *J. Exp. Nanosci*. **2016**, *11*, 226–238.
- [134] Alharthi, F. A.; Alghamdi, A. A.; Al-Zaqri, N.; Alanazi, H. S.; Alsyahi, A. A.; Marghany, A. El; Ahmad, N. Facile One-Pot Green Synthesis of Ag–ZnO Nanocomposites Using Potato Peel and Their Ag Concentration Dependent Photocatalytic Properties. *Sci. Rep*. **2020**, *10*, 1–14.
- [135] Kavitha, G.; Kumar, J. V.; Abirami, N.; Arulmozhi, R.; Siranjeevi, R.; Satish, R. Green Synthesis of Copper Oxide Nanoparticles Decorated with Graphene Oxide for Anticancer Activity and Catalytic Applications. *Arab. J. Chem*. **2020**.
- [136] Ullah, H.; Ullah, Z.; Fazal, A.; Irfan, M. Use of Vegetable Waste Extracts for Controlling Microstructure of CuO Nanoparticles: Green Synthesis, Characterization, and Photocatalytic Applications. *J. Chem*. **2017**.
- [137] Dupont, A.; Cusan, L.; Garon, M.; Labrie, F.; Li, C. H. β Endorphin: Stimulation of Growth Hormone Release in Vivo. *Proc. Natl. Acad. Sci. U. S. A*. **1977**, *74*, 358–359.
- [138] Dehghani, M.; Nadeem, H.; Raghuwanshi, V. S.; Mahdavi, H.; Banaszak Holl, M. M.; Batchelor, W. ZnO/Cellulose Nanofiber Composites for Sustainable Sunlight-Driven Dye Degradation. *ACS Appl. Nano Mater*. **2020**, *3*, 10284–10295.
- [139] León, E. R.; Rodríguez, E. L.; Beas, C. R.; Plascencia-Villa, G.; Palomares, R. A. I. Study of Methylene Blue Degradation by Gold Nanoparticles Synthesized within Natural Zeolites. *J. Nanomater*. **2016**.

- [140] Moradi, S.; Taghavi Fardood, S.; Ramazani, A. Green Synthesis and Characterization of Magnetic NiFe₂O₄@ZnO Nanocomposite and Its Application for Photocatalytic Degradation of Organic Dyes. *J. Mater. Sci. Mater. Electron.* **2018**, *29*, 14151–14160.
- [141] Stewart, A.; Zheng, S.; McCourt, M. R.; Bell, S. E. J. Controlling Assembly of Mixed Thiol Monolayers on Silver Nanoparticles to Tune Their Surface Properties. *ACS Nano.* **2012**, *6*, 3718–3726.
- [142] Amiri, M.; Etemadifar, Z.; Daneshkazemi, A.; Nateghi, M. Antimicrobial Effect of Copper Oxide Nanoparticles on Some Oral Bacteria and Candida Species. *J. Dent. Biomater.* **2017**, *4*, 347–352.
- [143] Renuga, D.; Jeyasundari, J.; Shakthi Athithan, A. S.; Brightson Arul Jacob, Y. Synthesis and Characterization of Copper Oxide Nanoparticles Using *Brassica Olerace* Extract for Its Antifungal Application. *Mater. Res. Express.* **2020**.
- [144] Manyasree, D.; Peddi, K. M.; Ravikumar, R. CuO Nanoparticles: Synthesis, Characterization and Their Bactericidal Efficacy. *Int. J. Appl. Pharm.* **2017**, *9*, 71–74.
- [145] Azam, A.; Ahmed, A. S.; Oves, M.; Khan, M. S.; Memic, A. Size-Dependent Antimicrobial Properties of CuO Nanoparticles against Gram-Positive and -Negative Bacterial Strains. *Int. J. Nanomedicine.* **2012**, *7*, 3527–3535.
- [146] Andualem, W. W.; Sabir, F. K.; Mohammed, E. T.; Belay, H. H.; Gonfa, B. A. Synthesis of Copper Oxide Nanoparticles Using Plant Leaf Extract of *Catha Edulis* and Its Antibacterial Activity. **2020**.
- [147] Kędziora, A.; Speruda, M.; Krzyżewska, E.; Rybka, J.; Łukowiak, A.; Bugła-Płoskońska, G. Similarities and Differences between Silver Ions and Silver in Nanoforms as Antibacterial Agents. *Int. J. Mol. Sci.* **2018**.
- [148] Ramalingam, B.; Parandhaman, T.; Das, S. K. Antibacterial Effects of Biosynthesized Silver Nanoparticles on Surface Ultrastructure and Nanomechanical Properties of Gram-Negative Bacteria Viz. *Escherichia Coli* and *Pseudomonas Aeruginosa*. **2016**.
- [149] Qais, F. A.; Shafiq, A.; Khan, H. M.; Husain, F. M.; Khan, R. A.; Alenazi, B.; Alsalmeh, A.; Ahmad, I. Antibacterial Effect of Silver Nanoparticles Synthesized Using *Murraya Koenigii* against Multidrug-Resistant Pathogens. *Bioinorg. Chem. Appl.* **2019**.

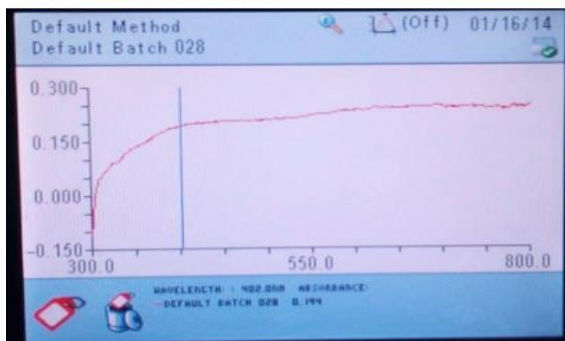
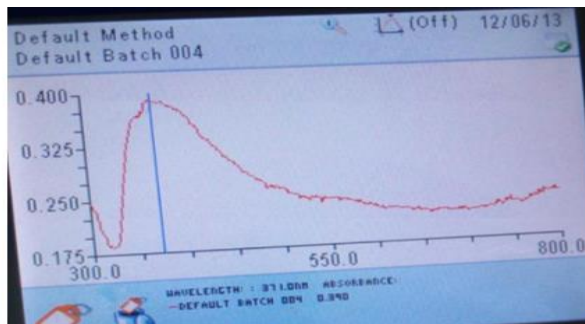
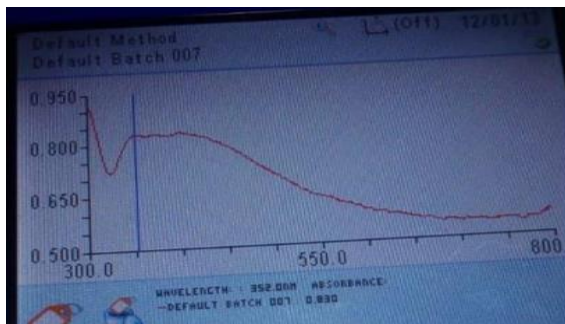
LIST OF APPENDICES



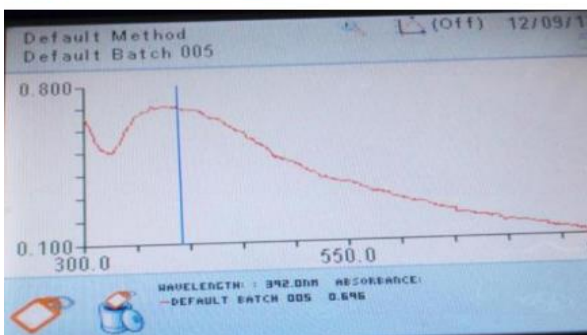
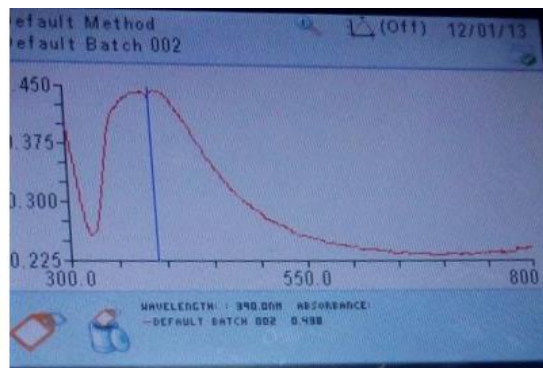
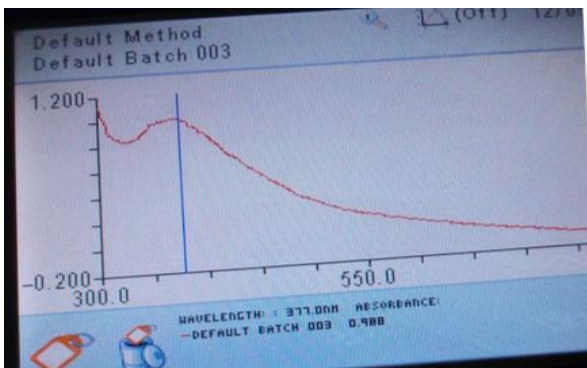
Appendix 1: Phyto-chemicals present in *Ocimum Lamiifolium* plant extract



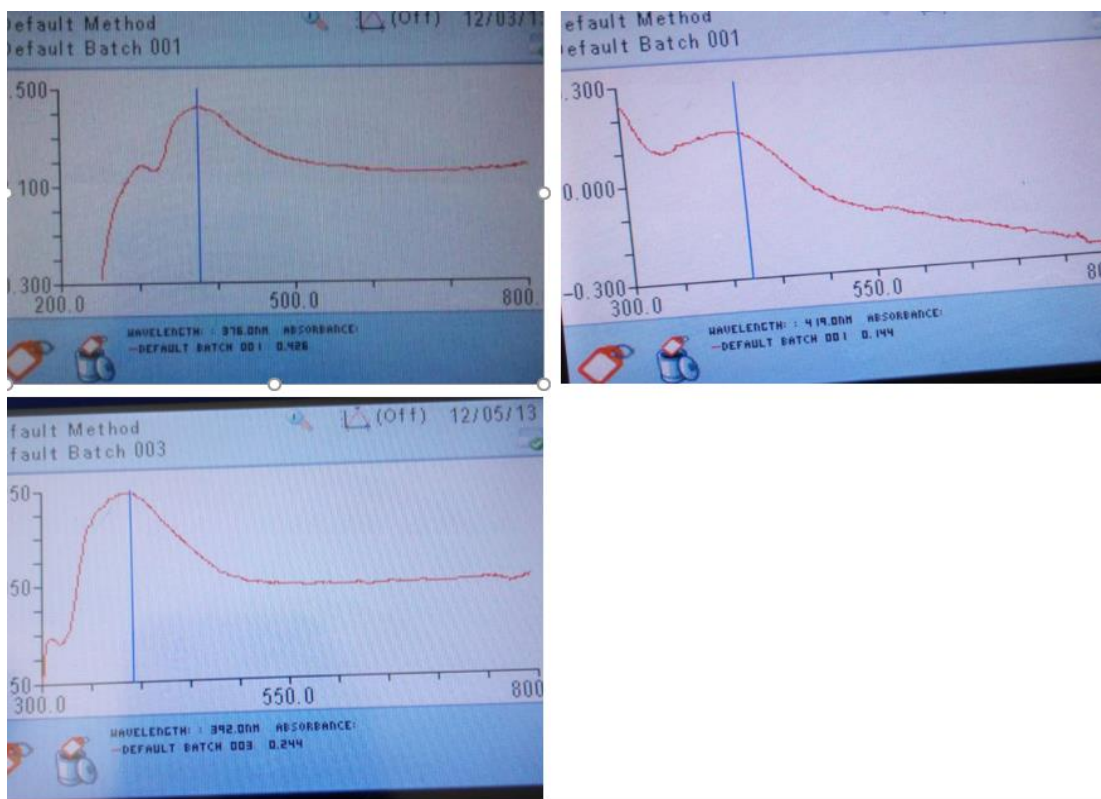
Appendix 2: Schematic diagram for (a) Preparation of plant extract (b) Synthesis of Ag/CuO NPs.



Appendix 3: Effect of different concentration copper nitrate trihydrate on UV-Vis absorption peak of Ag/CuO NCs.



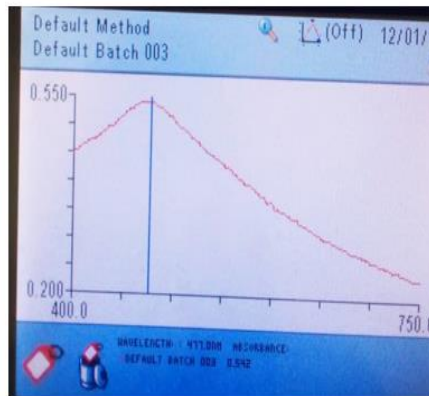
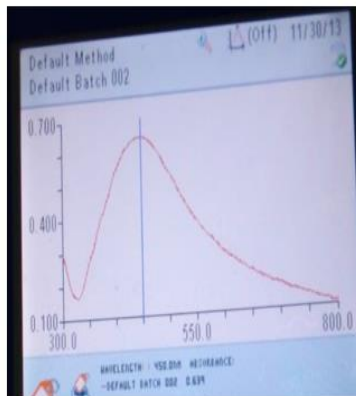
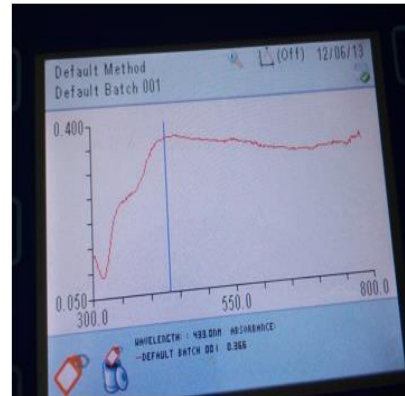
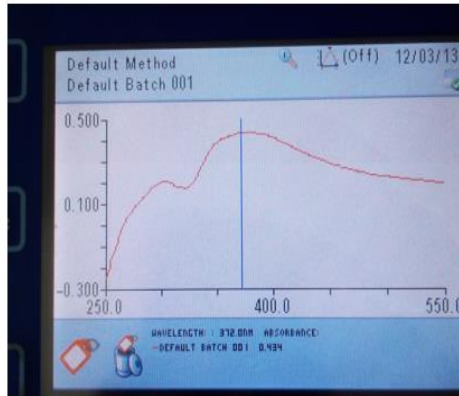
Appendix 4: Effect Volume of plant extract on synthesis of Ag/CuO NCs.



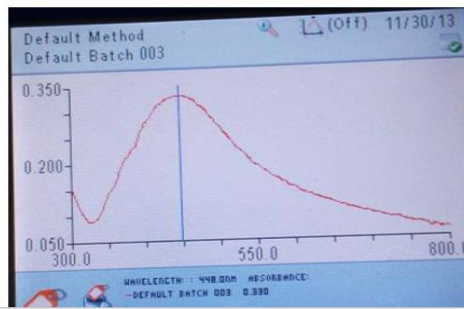
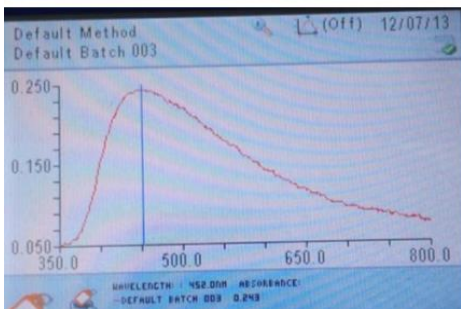
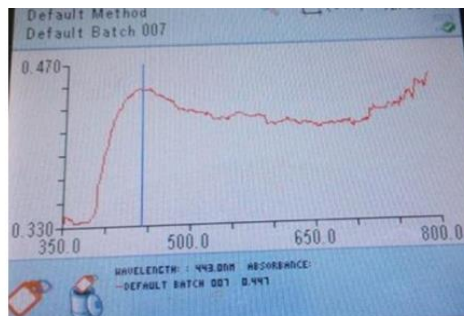
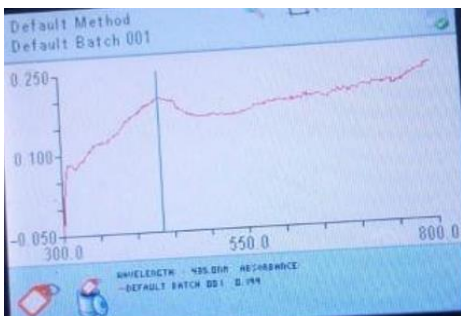
Appendix 5: Effect of concentration of Ag on synthesis of Ag/CuO NCs



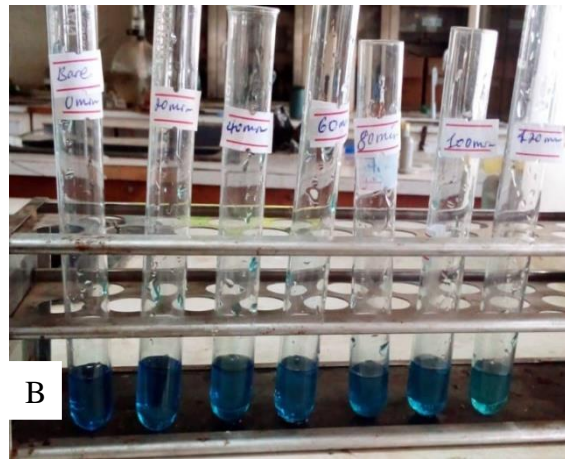
Appendix 6: Effect of pH on synthesis of Ag/CuO NCs



Appendix 7: Effect of temperature on synthesis of Ag/CuO NCs



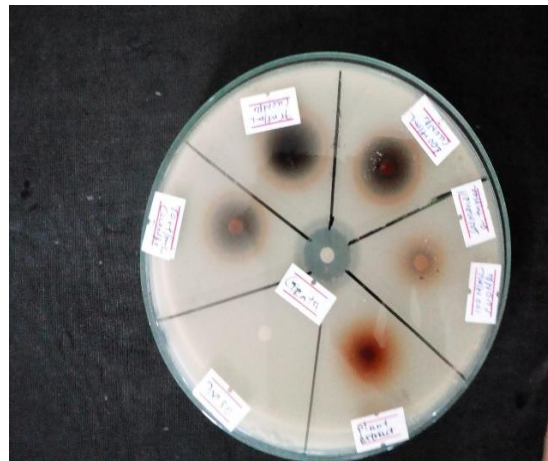
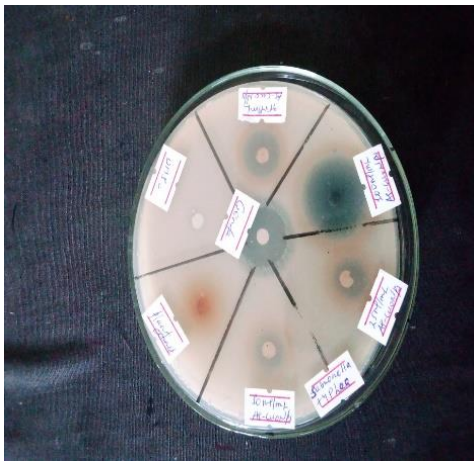
Appendix 8: Effect of reaction time on synthesis of Ag/CuO NCs



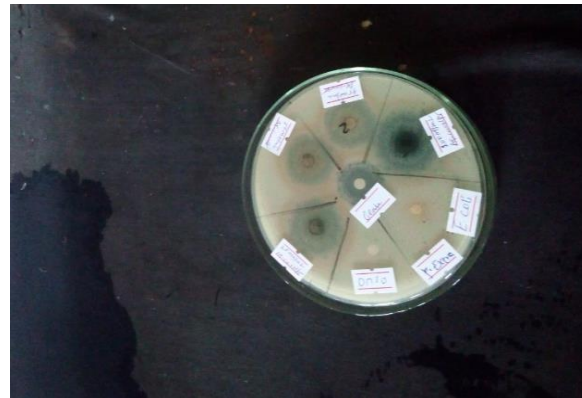
Appendix 9: Decolorization of MB (A) with Ag/CuO NCs (B) without catalyst.

CuO NPs

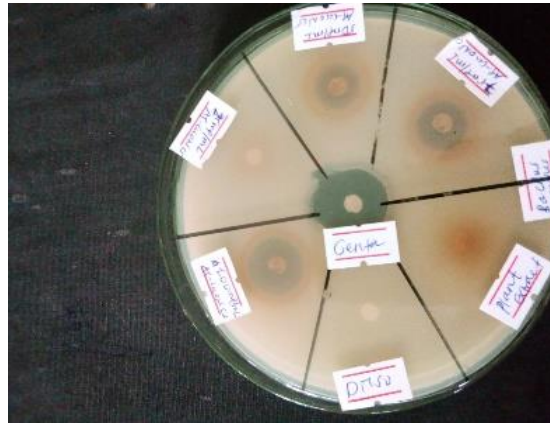
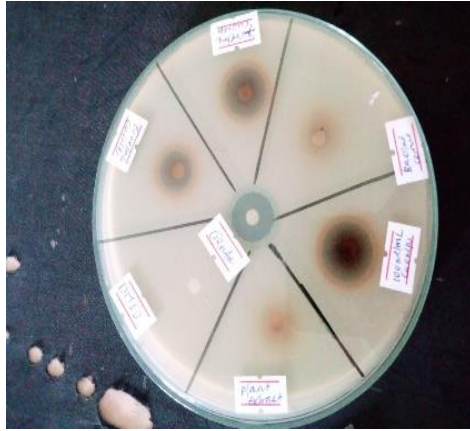
Ag/CuO NCs



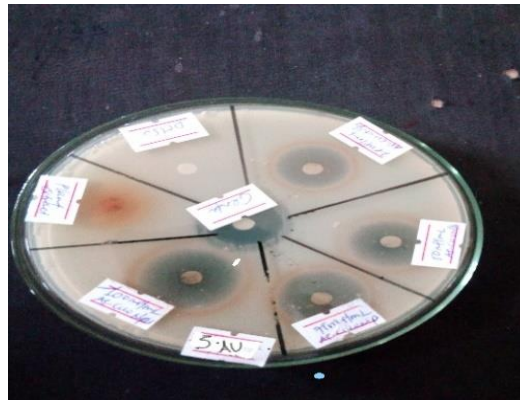
Salmonella typhi



E.coli

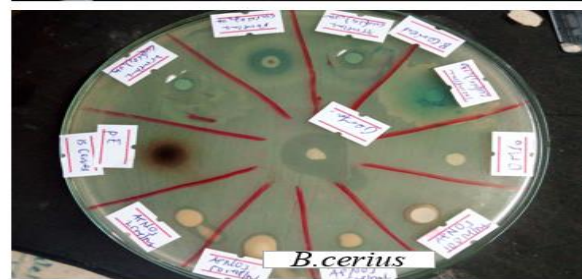
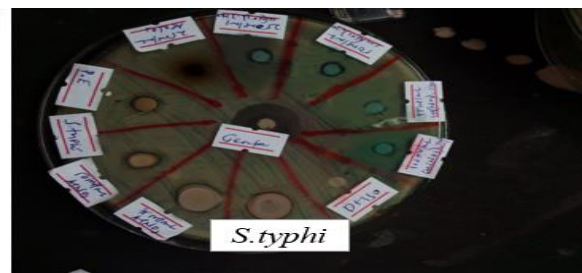
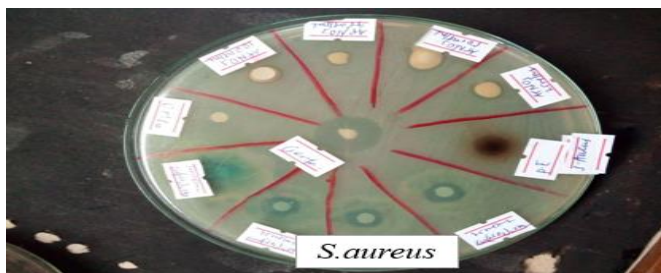


B. cereus



S. aureus

Appendix 10(A): Antibacterial activity of CuO NPs and Ag/CuO NCs



Appendix 10 (B): Antibacterial activity of bulk $\text{Cu}(\text{NO}_3)_2 \cdot 3\text{H}_2\text{O}$ and AgNO_3

Appendix 10 B (Table A): Antibacterial activity of bulk $\text{Cu}(\text{NO}_3)_2 \cdot 3\text{H}_2\text{O}$ and AgNO_3

Concentration of $\text{Cu}(\text{NO}_3)_2 \cdot 3\text{H}_2\text{O}$ and AgNO_3 (mg/ml)		Zone of inhibition (mm)			
		<i>S. aureus</i>	<i>S. typhi</i>	<i>E. coli</i>	<i>B. cereus</i>
100	Cu^{+2}	16	13	14	15.5
	Ag+	15.25	12	13.75	15.5
75	Cu^{+2}	14	12.5	13	11
	Ag+	14	11	12.25	11
50	Cu^{+2}	12	12	12	10.5
	Ag+	11	10.5	10	9
25	Cu^{+2}	7.5	NI	NI	7.5
	Ag+	NI	NI	NI	7.5
Plant extract		10	7	8	9
DMSO		NI	NI	NI	NI
Gentamicin		20	20.3	21.5	23.5

NI= No inhibition